ACSNANO

www.acsnano.org

ARTICLE

Fully Biodegradable and Long-Term Operational Primary Zinc Batteries as Power Sources for Electronic Medicine

Xueying Huang, Hanqing Hou, Bingbing Yu, Jun Bai, Yanjun Guan, Liu Wang, Kuntao Chen, Xibo Wang, Pengcheng Sun, Yuping Deng, Shangbin Liu, Xue Cai, Yu Wang, Jiang Peng, Xing Sheng, Wei Xiong,* and Lan Yin*

Cite This: *ACS Nano* 2023, 17, 5727−5739

Read Online

ACCESS | Metrics & More | Article Recommendations | Supporting Information

ABSTRACT: **Given the advantages of high energy density and easy deployment, biodegradable primary battery systems remain as a promising power source to achieve bioresorbable electronic medicine, eliminating secondary surgeries for device retrieval. However, currently available biobatteries are constrained by operational lifetime, biocompatibility, and biodegradability, limiting potential therapeutic outcomes as temporary implants. Herein, we propose a fully biodegradable primary zinc−molybdenum (Zn−Mo) battery with a prolonged functional lifetime of up to 19 days and desirable energy capacity and output voltage compared with reported primary Zn biobatteries. The Zn−Mo battery system is shown to have excellent biocompatibility and biodegradability and can significantly promote Schwann cell proliferation and the axonal growth of dorsal root ganglia. The biodegradable battery module with 4 Zn−Mo cells in series using gelatin electrolyte accomplishes electrochemical generation of signaling molecules (nitric oxide, NO) that can modulate the behavior of the cellular network, with efficacy comparable with that of conventional power sources. This work sheds light on materials strategies and fabrication schemes to develop high-performance biodegradable primary batteries to achieve a fully bioresorbable electronic platform for innovative medical treatments that could be beneficial for health care.**

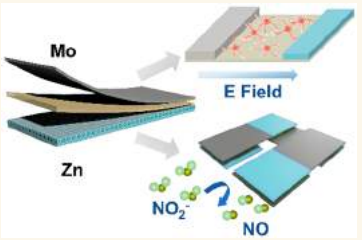

KEYWORDS: *fully biodegradable battery, primary zinc battery, electric field, electronic medicine, nitric oxide delivery*

Biodegradable electronic medicine is an emerging type of device platform that can modulate organ functions, improve therapeutic outcomes, and resorb safely in physiological environments after treatment windows, eliminating secondary surgeries for device retrieval. Demonstrated systems include bioresorbable cardiac pacemakers,[1] devices promoting nerve and neuromuscular regeneration,[2−4] piezoelectric stimulators for cartilage regeneration,[5] *etc.* Although current advances show great promise, the associated biodegradable power supply components remain the key challenge to achieving miniaturized and robust functional systems. Several strategies have been proposed to tackle the problem,[6] including biodegradable energy storage systems (batteries[7−12] and supercapacitors[13−15]), biodegradable energy transfer devices based on inductive coupling[16] and photovoltaics,[17,18] and biodegradable power harvesting devices (triboelectric devices,[19] piezoelectric harvesters,[20] *etc.*). In particular, biodegradable primary batteries have attracted great attention due to their high energy density, easy deployment, and lower constrains in implantation locations. The biodegradable feature could eliminate unnecessary materials retention after operational time frames and avoid potential hazardous constituents present in conventional lithium-based batteries that are often adopted in commercial implantable electronics.[21]

Biodegradable batteries have been realized with biocompatible and degradable metals,[7,8] metal oxides,[10] and bioorganic materials.[22] Dissolvable metals including magnesium (Mg), zinc (Zn), molybdenum (Mo), iron (Fe), tungsten (W),[7] and magnesium-based alloys[23−25] have been proposed as potential electrode materials for primary batteries because of desirable electrical conductivity, electrochemical activity, biocompatibility, and biodegradability. For instance, researchers have achieved biodegradable primary batteries based on Mg anodes such as Mg−Fe, Mg−Mo, and Mg−W cells.[7,8,26] However, Mg

Received: December 7, 2022
Accepted: March 2, 2023
Published: March 10, 2023

https://doi.org/10.1021/acsnano.2c12125
ACS Nano 2023, 17, 5727−5739

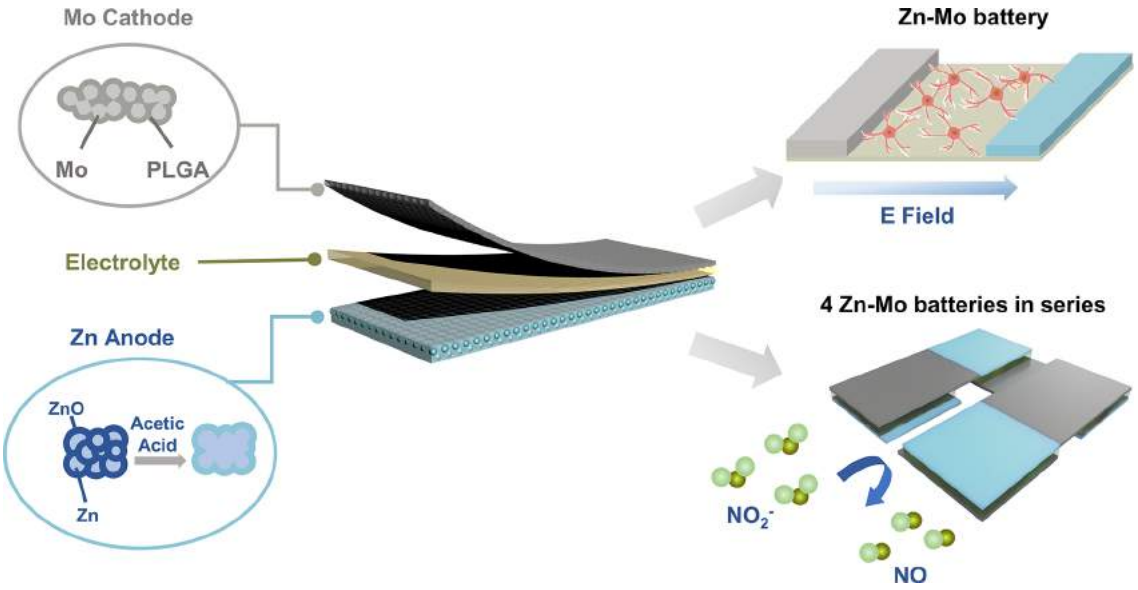

Figure 1. Schematic illustration of the fully biodegradable primary zinc−molybdenum (Zn−Mo) battery. The battery comprises Mo particle electrodes as the cathode, Zn particle electrodes sintered by acetic acid as the anode, and normal saline solutions or hydrogels as the electrolyte. The electric field provided by the Zn−Mo battery can stimulate the growth of dorsal root ganglia (DRG). Putting Zn−Mo batteries in series can promote the output voltage and drive electrochemical reactions to produce signaling molecules such as nitric oxide (NO) to modulate cellular behavior.

often undergoes intense side reactions with aqueous electrolytes due to its bioactivity, which limits the operational lifetime and causes extra hydrogen production. Zn represents an alternative candidate anode material with suppressed adverse reactions and has a theoretical volume specific capacity up to 5822 mAh cm^{-3}, low equilibrium potential (−0.763 V *vs* standard hydrogen electrode), and high hydrogen evolution potential.[27−29] Zn also plays an important role in biological processes, including endocrine homeostasis, hippocampus function, bone growth, *etc.*[30] The National Institutes of Health (NIH) Office of Dietary Supplements (ODS) of the U.S. recommends a daily Zn intake of 12 mg for adults.[31]

Although biobatteries with zinc anodes have been investigated coupling with cathode materials such as gold (Au),[32,33] platinum (Pt),[34] or carbon nanotubes,[35,36] fully biodegradable Zn battery systems have rarely been reported. Dissolvable metals, alloys, and oxides (*e.g.*, Fe,[8,26] Mo,[7] W,[7] iron−manganese alloy (FeMn),[4] and molybdenum trioxide (MoO_3)[10]) have been employed as cathode materials in Mg biobatteries with great biocompatibility and performance, which offers material strategies for biodegradable cathodes in Zn batteries. In addition, gastric juice (pH ∼2) consisting of hydrochloric acid, potassium chloride, and sodium chloride is often adopted as the electrolyte for Zn biobattery to improve the output power.[9,34,37] Different strategies have been proposed to achieve enhanced performance in near neutral environments, including the introduction of solid or gel electrolytes, the construction of 3D porous anodes, surface optimization, *etc.*[28] For example, Zn biobatteries with desirable characteristics have been realized in near neutral electrolytes (*e.g.*, 0.9% NaCl saline, gelatin−silk protein films with 2 M of $ZnSO_4$ and 0.1 M of $MnSO_4$) with Zn electrodes sintered from nanoparticles at room temperature.[32,35,36] Nevertheless, the operational lifetime of reported zinc biobattery is limited to around 8 days. Further materials strategies are critical to extend the functional windows to provide sufficient power support to ensure satisfied outcomes for electronic medicine, as tissue regeneration or function restoration could take weeks to months.

Here, we develop a fully biodegradable primary battery system composed of a Zn anode and Mo cathode materials (Figure 1). By sintering of Zn nanoparticles using acetic acid at room temperature, the specific surface area of the Zn electrode can be effectively improved compared with the foil format. Mo is selected as the cathode materials due to desirable degradation rates, excellent electrical conductivity, and biocompatibility,[7,38,39] enabling fully degradable Zn biobatteries. The dissolution rates of Mo thin films could achieve 7 × 10^{-4} μm/h in pH 7.4 at 37 °C, and the tolerable upper intake level of Mo for adults above 19 years old is 2000 μg daily.[31,38] The discharge lifetime of Zn−Mo battery in aqueous electrolyte up to 19 days is achieved, which exceeds the lifetime of most reported primary biobatteries based on Mg or Zn anodes. Zn−Mo batteries also reveal desirable biocompatibility and biodegradability in biological environments. The electric field supplied by Zn−Mo batteries is shown to promote the proliferation of Schwann cells and the axonal growth of dorsal root ganglia (DRG) (Figure 1). Zn−Mo batteries have also been demonstrated as a power source to drive the electrolysis of nitric oxide (NO) production to regulate the behavior of cells (Figure 1). The work offers another path toward the development of fully biodegradable primary batteries with prolonged lifetime and sheds light on power solutions for biodegradable and self-powered electronic medicine.

RESULTS AND DISCUSSION

Materials Strategies and Battery Performance. Fully biodegradable primary Zn−Mo batteries consist of Zn and Mo electrodes with normal saline (0.9 wt % NaCl, pH ∼7) or hydrogel (gelatin with 9 wt % NaCl) as the electrolyte (Figure 1). Zn electrodes are achieved by sintering the nanoparticles at room temperature. Due to spontaneous oxidation, a thin layer of oxide is present on the surface of Zn particles, which affects

https://doi.org/10.1021/acsnano.2c12125
ACS Nano 2023, 17, 5727−5739

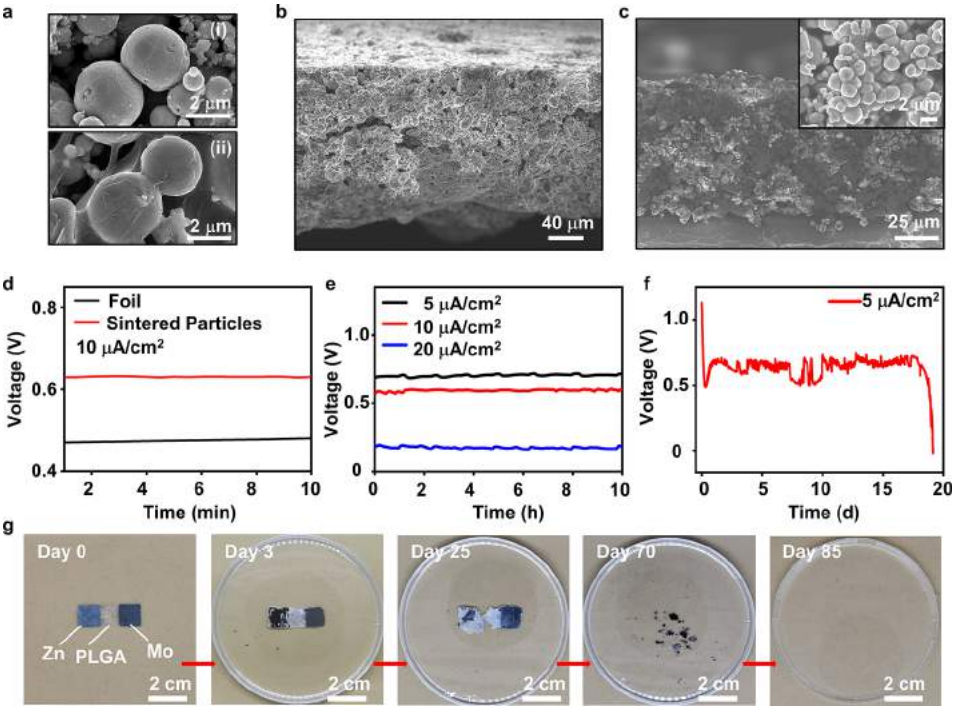

Figure 2. Electrode materials and discharge characteristics of the fully degradable primary Zn−Mo battery. (a) Scanning electron microscopy (SEM) images of Zn electrode before (i) and after (ii) room temperature sintering. (b) SEM image of the cross section of Zn electrode. (c) SEM image of the cross section of Mo electrode. Inset indicates the enlarged view of Mo electrode. (d) Discharge behavior of Zn−Mo batteries based on foils and sintered particles. (e) Discharge behavior of Zn−Mo batteries with sintered particles electrodes with different current densities. (f) Long-term discharge behavior of Zn−Mo batteries with sintered particles electrodes (current density: 5 μA/cm^2). (g) Dissolution of Zn−Mo battery at various stages after immersion in PBS (pH 7.4) at 37 °C.

the conductivity of Zn particle network.[40] The use of acetic acid solutions can gently remove the surface oxide layer, exposing the metallic component without excessive corrosion. In the mild acidic environment, the self-exchange of Zn and Zn ions could occur between particles and acetic acid solutions, through the dissolution of Zn metal and the deposition of Zn ions.[41]

Figure 2a shows the scanning electron microscopy (SEM) images of Zn particles before and after acetic acid sintering. Zn particles form an interconnected network after sintering, and a significant decrease in resistivity from 20 MΩ/cm to 2 Ω/cm is achieved. A thin layer of Zn oxide could be developed on the newly formed surface of the porous electrodes to prevent further oxidation. Mo particles are treated by hydrochloric acid (HCl) solutions to remove the surface oxide layer and mixed with the biodegradable polymer poly(lactic-*co*-glycolic) acid (PLGA) to obtain the Mo electrode. The cross sections of Zn and Mo electrodes are shown in Figure 2b,c, and the thicknesses are around 150 and 65 μm, respectively. Electrochemical impedance spectroscopy (EIS) measurements of Zn and Mo electrodes are carried out in normal saline, phosphate-buffered saline (PBS, pH ∼7.4), and simulated gastric juice (pH ∼2) to investigate the impedance characteristics of foil (20 μm) and particle electrodes. As shown in Figure S1, the impedances of particle electrodes are mostly smaller than those of the foil electrodes, especially in the low frequency region, which is likely resulting from the improved effective surface area based on metallic particles. In addition, highly acidic electrolytes such as gastric juice tend to lower the interfacial impedance of the Zn electrodes.

The discharge performance of Zn−Mo batteries is tested with normal saline as the electrolyte. The reaction occurring on the anode is expected to be the oxidation of Zn:[32]

$$Zn_{(s)} \leftrightarrow Zn^{2+}_{(aq)} + 2e^- \quad (1)$$

Side reactions could also take place as Zn reacts directly with the electrolyte, accompanied by an increase of pH near the anode electrode. Byproducts such as Zn hydroxide or zinc oxide (ZnO) could form as a coating layer on the surface of Zn electrode,[41] which is soluble slowly in the aqueous environments such as normal saline.[42]

$$Zn + 4OH^- \leftrightarrow Zn(OH)_4^{2-} + 2e^- \leftrightarrow ZnO + 2OH^- + H_2O + 2e^- \quad (2)$$

At the cathode, hydrogen evolution (eq 3) or oxygen reduction (eq 4) could occur:[32,43]

$$2H_2O + 2e^- \leftrightarrow H_2 + 2OH^- \quad (3)$$

$$O_2 + 2H_2O + 4e^- \leftrightarrow 4OH^- \quad (4)$$

The discharge behavior of batteries in normal saline appears in Figure 2d. Under the same discharge current density (10 μA/cm^2), batteries with electrodes fabricated from particles demonstrate greater output voltage around 0.6 V compared with batteries with foil electrodes, which is similar to the output voltage obtained in gastric acid solutions (pH ∼2) using foil electrodes (Figure S2). The results suggest that the porous electrode based on metallic particles can ensure desirable output voltage in near neutral environments, and electrodes based on particles are therefore used for the rest of the studies unless otherwise specified. The discharge behavior

https://doi.org/10.1021/acsnano.2c12125
ACS Nano 2023, 17, 5727−5739

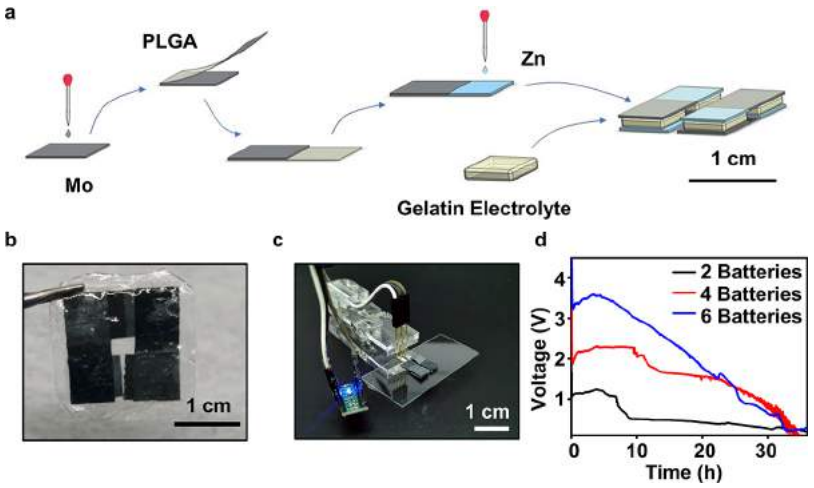

Figure 3. Fully biodegradable primary Zn−Mo batteries connected in series and associated performance. (a) Schematic illustration of the fabrication process of integrating 4 Zn−Mo cells in series (Zn−Mo battery module) with gelatin as the electrolyte. (b) Photo of serial-connected Zn−Mo battery module. (c) Blue LED (threshold voltage ∼2.3 V) powered by 4 Zn−Mo cells in series. (d) Discharge behavior of serial-connected Zn−Mo batteries with gelatin as the electrolyte. Discharge current: 40 μA/cm^2.

with different current densities of Zn−Mo batteries appears in Figure 2e. The output voltage decreases as the current density increases. The corresponding calculated power densities are summarized in Figure S2a. A power density of 6 μW/cm^2 is achieved with a discharge density of 10 μA/cm^2 in normal saline. The influences of electrolytes on the discharge behavior of Zn−Mo batteries are investigated, and the results are given in Figure S2b,c. Strong acidic electrolyte can reduce charge transfer resistance on the electrode surface and improve the output characteristic, which however could also lead to severe side reactions and the rapid consumption of Zn anode materials. PBS can serve as an alternative electrolyte, but the presented phosphate ions tend to form insoluble zinc phosphates on the electrode surface and hinder long-term operation. The prolonged lifetime of Zn−Mo battery of approximately 19 and 12 days is demonstrated with a discharge current density of 5 and 10 μA/cm^2 in normal saline, respectively (Figures 2f and S2d), which exceeds the reported functional time frames of most biodegradable primary Mg and Zn batteries. The extended operational window is attributed to the relatively slow side reactions due to the coating of associated byproducts (*e.g.*, Zn hydroxide and ZnO) on the electrode surface. It is worth mentioning that the constant spalling and precipitation of Zn oxides and Zn hydroxides could introduce minor instability of the discharge curve, as shown in Figure 2f. Furthermore, the degradation rates of metallic Mo are slower than that of Zn in aqueous solutions. Thus, the degradation of Zn electrodes often determines the operational time frame of the battery. Compared with previously reported Zn primary biobatteries, the fully biodegradable Zn−Mo cells demonstrate a prolonged lifetime, high voltage, and comparable energy capacity (Table S1).

The degradation process of a Zn−Mo battery fabricated on a PLGA substrate in PBS at 37 °C at various stages is shown in Figure 2g. The electrodes gradually dissolve overtime and the PLGA substrate degrades through swelling, hydrolysis, and depolymerization. Obvious disintegration of electrodes and substrate materials occurs around 25 days. The leftover of traces of metallic electrodes are observed after 70 days, and the constituent materials of Zn−Mo batteries completely disappear after 85 days. Based on reported corrosion rates of Zn and Mo under different pH environments, strong acidic (pH <2) or alkaline solutions (pH >12) are expected to significantly expedite the degradation of Zn−Mo batteries.[38,44]

Zn and Mo electrodes achieved with metallic particles and polymeric encapsulation endow the battery with a certain level of flexibility. As shown in Figure S3a, fabricated electrodes can be rolled to a glass rod (5 mm in diameter) and remain conductive, demonstrating desirable flexibility. The mechanical properties of Zn and Mo electrodes are evaluated by tensile tests, and the results appear in Figure S3b−d and Table S2. The elongation at break of Zn and Mo electrodes is more than 30%. The Young's modulus of Zn and Mo electrodes is 0.251 ± 0.092 and 0.509 ± 0.267 MPa, respectively, greater than those of pure PLGA (0.012 MPa) or gelatin electrolyte (0.0235 MPa at 90% water content).[45] The battery is expected to be able to adapt to the movements of the body without extremely large deformation. Nevertheless, repeated bending could create microcracks in the electrodes and provide more pathways for the infiltration of body fluids, resulting in accelerated degradation. Optimization of battery size, configuration, and encapsulation polymers could further improve flexibility.

To promote the output performance, a fully biodegradable primary battery module connecting 4 Zn−Mo cells in series using biodegradable Mo powder slurry has been achieved (Figure 3a). Gelatin, a biodegradable and biocompatible natural hydrogel that has excellent formability with salt concentrations of wide ranges, is adopted as the electrolyte to facilitate battery assembly. Concentrated saline (9 wt % NaCl, ten times that of normal saline) is incorporated in the gel electrolyte to further improve the discharge behavior. The photograph of the battery module appears in Figure 3b. As shown in Figure 3c, a blue LED (threshold voltage ∼2.3 V) can be lit up by the battery module with 4 Zn−Mo cells. The output voltage of the battery module can be improved by increasing the number of batteries in series, and the voltage of 1, 2.2, and 3.6 V are realized with serial connection of 2, 4, and 6 batteries, respectively, with a discharge current density of 40 μA/cm^2 (Figure 3d). The gradual decrease in output voltage is probably due to the dehydration of gel electrolyte exposed in air and the insufficient dissipation of dissolution byproducts

https://doi.org/10.1021/acsnano.2c12125
ACS Nano 2023, 17, 5727−5739

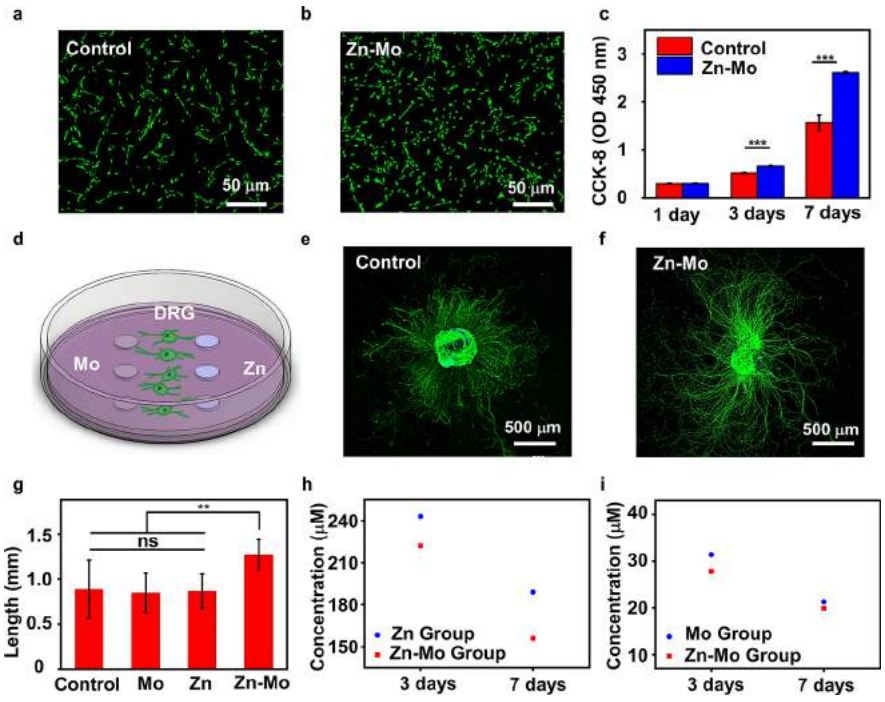

Figure 4. Influence of primary Zn−Mo batteries on the growth behavior of DRG and Schwann cells. (a) Growth behavior of Schwann cells after 3 days of culturing in the control group. (b) Growth behavior of Schwann cells after 3 days of culturing in the Zn−Mo group. (c) Proliferation assay of Schwann cells using the CCK-8 test. (d) Schematic illustration of DRG cocultured with Zn−Mo batteries. (e) Confocal microscope image of the DRG of the control group after 7 days of culturing. (f) Confocal microscope image of the DRG of Zn−Mo group after 7 days of culturing. (g) Statistical analysis of the averaged neurite length of DRG of the control, Mo, Zn, and Zn−Mo groups. Data are shown as means ± standard deviations; $n = 3$ independent experiments per group. The SPSS software package (version 23.0) is used for the statistical analysis, followed by one way ANOVA ($P < 0.01$, ***$P < 0.001$). (h) ICP-MS analysis results of Zn release in cell culture medium. (i) ICP-MS analysis results of Mo release in cell culture medium.**

within the gel matrix which could hinder further discharge behavior. Nevertheless, these results offer potential strategies to promote the output voltage and discharge current density of biodegradable Zn−Mo batteries.

Zn−Mo Batteries Offering Electric Fields to Promote Cell Growth. To evaluate the biocompatibility and the feasibility as a power source for electronic medicine, Zn−Mo primary batteries are cultured with Schwann cells and DRG. Schwann cells represent important active glial cells in peripheral nerves and play an important role in the survival and regeneration of damaged axons. An extra thin layer (1 μm) of PLGA is coated on the surface of Zn and Mo electrodes to control the release rate of metallic ions. The fluorescent images of Schwann cells cocultured with Zn−Mo batteries and the control group (without Zn−Mo batteries) after 3 days appear in Figure 4a,b, and the proliferation assessment based on CCK-8 assay is given in Figure 4c. The results suggest that the proliferation of Schwann cells is greatly promoted in the presence of Zn−Mo batteries, while the extracts of Zn or Mo electrodes soaking in PBS do not show an obvious difference in promoting cell growth compared with the control group (Figure S4a). The release of Zn and Mo ions in the culture medium on day 3 is analyzed by inductively coupled plasma-optical emission spectrometry (ICP-OES), and the concentrations of Zn and Mo are in the range of 15−175 and 5−165 μM, respectively. The wide deviation of detected ion concentration is probably due to varied effectiveness of the thin PLGA encapsulation. Nevertheless, no significant adverse effects are observed within the range of measured ion concentrations. The electrode materials and open circuit voltage of Zn−Mo batteries also retain after coculturing with Schwann cells, suggesting a stable electric field could be provided through cell proliferation. In all, the results demonstrate desirable biocompatibility of Zn−Mo batteries with Schwann cells, and the electric field provided by Zn−Mo batteries could effectively promote cell growth.

The influence of the Zn−Mo battery on axonal growth of DRG is also investigated, and the experimental setup appears in Figure 4d. The fluorescence microscopic images after 7 days of culturing of the Zn−Mo, Zn, Mo, and control groups are given in Figure 4e,f and Figure S4b,c. The statistical results of the axon length are quantified by ImageJ software, and the results appear in Figure 4g. The results suggest that Zn and Mo electrodes possess desirable biocompatibility and Zn−Mo batteries significantly promote axonal growth, consistent with previously reported results with Mg batteries.[4] The electric field provided by the primary Zn−Mo battery could promote calcium activity and stimulate brain-derived neurotrophic factor (BDNF) and associated tropomyosin kinase B (TrkB) in the neuronal cell body, which could subsequently upregulate the expression of regeneration-related phospholipids by boosting cyclic adenosine monophosphate (cAMP) pathways, assisting the axonal growth.[4,46] ICP-OES analysis is performed on DRG culture medium, and the ion concentrations of Zn and Mo are in the range of 150−250 and 20−30 μM, respectively (Figure 4h,i). To summarize, Zn−Mo batteries could potentially work as electronic medicine directly by offering an electric field to promote the proliferation of Schwann cells and the axonal growth of DRG, which is beneficial for peripheral nerve regeneration.

https://doi.org/10.1021/acsnano.2c12125
ACS Nano 2023, 17, 5727−5739

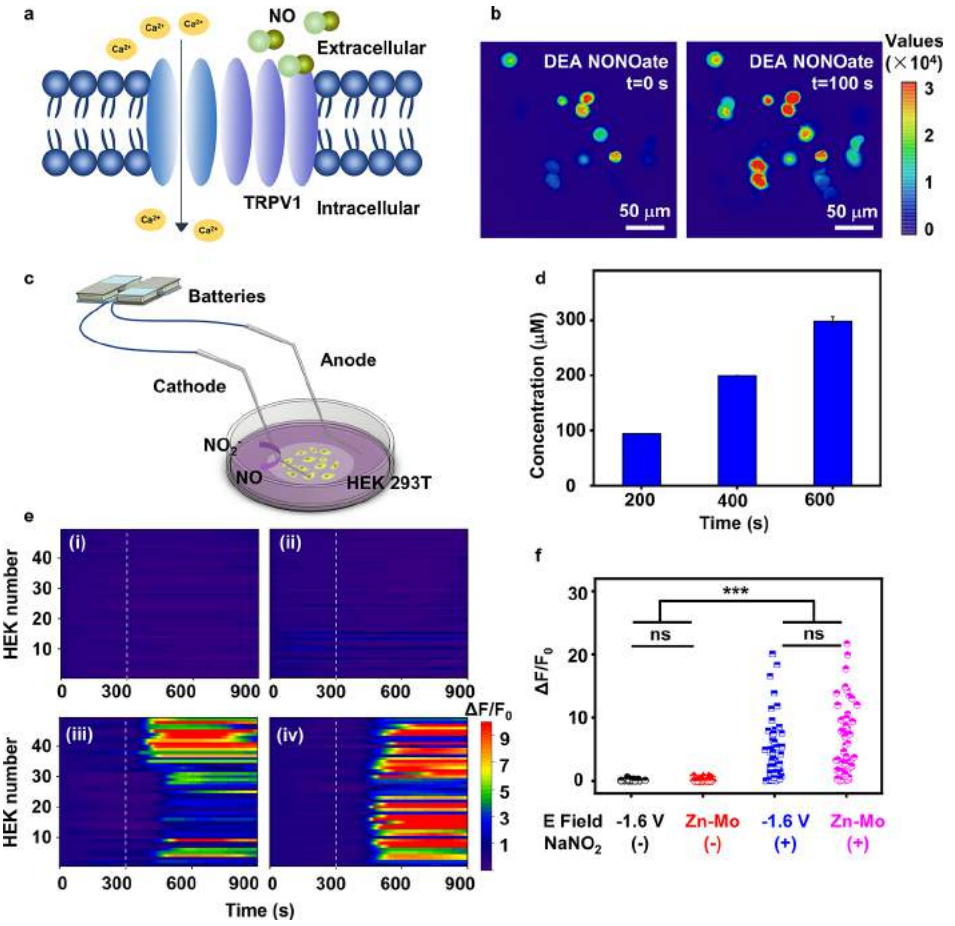

Figure 5. Electrochemical NO generation driven by the biodegradable Zn−Mo battery module (4 cells in series). (a) Schematic diagram of Ca^{2+} influx through TRPV1 mediated by NO. (b) Time-lapse images of Ca^{2+} responses in HEK 293T cells expressing TRPV1 (TRPV1$^+$) upon DEA NONOate (10 mM) infusion. (c) Schematic illustration of electrochemical NO delivery achieved by the Zn−Mo battery module. (d) Electrochemical generation of NO driven by the Zn−Mo battery module. (e) Individual GCaMP6s fluorescence traces for TRPV1$^+$ cells (n = 50 cells for each condition): (i) without $NaNO_2$ (−) and with an electric field of −1.6 V provided by a potentiostat; (ii) without $NaNO_2$ (−) and with an electric field provided by a Zn−Mo battery module; (iii) with 10 mM $NaNO_2$ (+) and with an electric field of −1.6 V provided by a potentiostat; (iv) with 10 mM $NaNO_2$ (+) and with an electric field provided by a Zn−Mo battery module. Electric fields are applied at 300 s (white dash line). (f) Statistical results of the maximum fluorescence intensity of TRPV1$^+$ cells. The SPSS software package (version 23.0) is used for the statistical analysis, followed by one way ANOVA (*P < 0.001).**

Zn−Mo Battery Module as a Power Source to Deliver NO and Modulate Cell Behavior. The biodegradable battery module consisting of 4 Zn−Mo batteries with gelatin electrolyte is used to investigate the feasibility as the power device to deliver NO on demand and modulate cell behavior. As an important signaling molecule,[47,48] controlled NO delivery in biological systems remains a challenge due to its short half-life.[49,50] In situ NO release has been achieved through light triggering and electrochemical electrolysis for treating spinal cord injury (SCI)[51] and regulating biological functions.[49] Exploring biodegradable batteries as potential power sources could offer a candidate platform for the controlled release of NO.

To investigate the effects of NO on cellular behavior, human embryonic kidney (HEK) 293T cells are selected in which DNA fragments are transferred by human adenovirus type 5. Transient receptor potential vanilloid family membrane 1 (TRPV1)[52,53] is chosen for the characterization of NO-mediated signal transduction, since it has been demonstrated to mediate NO-induced nociception in peripheral nervous system of mouse response to NO stimulation.[54,55] The calcium indicator GCaMP6s plasmid is cotransfected to observe NO associated response.[56] As illustrated in Figure 5a, when TRPV1 on the cell membrane is stimulated by NO, calcium channels are simultaneously opened, and extracellular calcium ions flow into the cell and combine with the indicator, resulting in changes in intracellular fluorescence intensity.[49] The improved influx of calcium ions is observed after adding NO donor DEA NONOate (10 mM) as shown in Figure 5b, demonstrating that HEK 293T cells are successfully transfected with TRPV1 and the GCaMP6s plasmids. Nitrite (NO_2^-) or nitrate (NO_3^-) is present in biological systems and could serve as substrates to generate NO by an enzymatic denitrification reaction.[57−59] Sodium nitrite ($NaNO_2$) has been used for electrolytic NO generation.[49] The biodegradable Zn−Mo module (serial connection of 4 cells) is therefore used to induce electrolysis in $NaNO_2$ solutions (10 mM) and generate NO to modulate the behavior of HEK 293T cells (Figure 5c), evaluating the potential of Zn−Mo batteries as a power source for electronic medicine with NO delivery.

The feasibility of electrochemical NO generation is first verified in Tyrode's solution with different concentrations of $NaNO_2$. NO can be generated by the reduction of nitrites:[60]

https://doi.org/10.1021/acsnano.2c12125
ACS Nano 2023, 17, 5727−5739

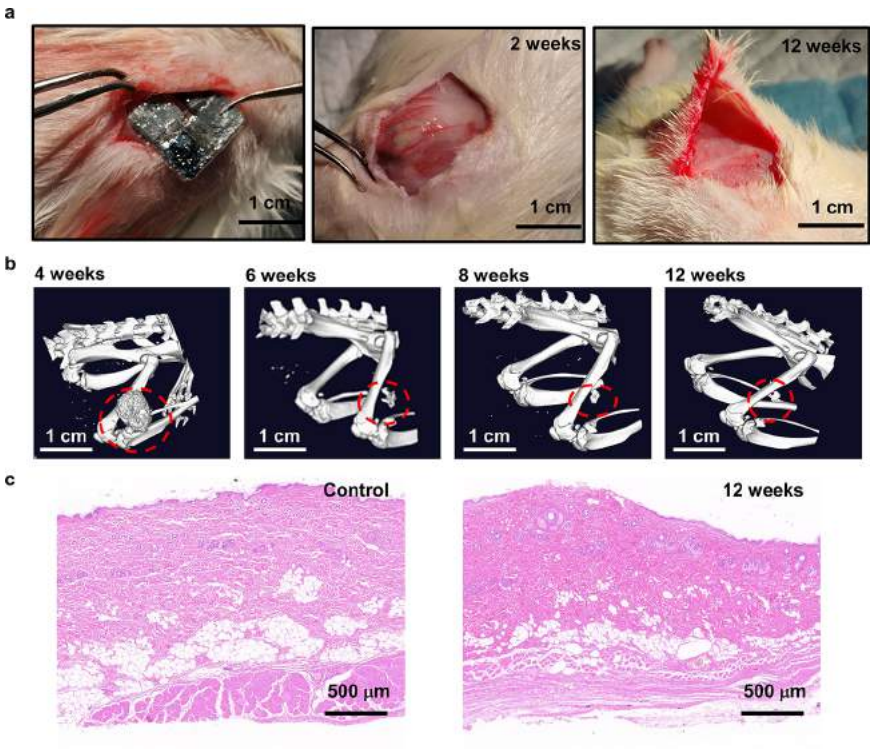

Figure 6. Biocompatibility and biodegradability studies of Zn−Mo batteries. (a) Images of batteries implanted in the subdermal region of SD rats at different stages of degradation over 12 weeks. (b) Three-dimension-rendered CT images of SD rats over 12 weeks after the implantation of the Zn−Mo battery (red dash line indicates the implantation site). (c) Hematoxylin and eosin (H&E) staining images of tissues surrounding the implantation regions; n = 3 independent experiments.

$$2NO_2^- + 2e^- + 4H^+ \leftrightarrow 2H_2O + 2NO \quad (5)$$

The cyclic voltammetry (CV) curves are measured by a two-electrode configuration, and the results are given in Figure S5. In the presence of 10 mM $NaNO_2$, response current increases significantly at around −1.6 V and reaches the reduction peak at approximately −1.84 V *versus* Pt electrode, while only broad redox characteristics are observed in similar voltage range in the solution without $NaNO_2$ (Figure S5a), suggesting a potential voltage window for electrochemical NO production which is comparable with the previous report.[49] The reduction peaks shift negatively with greater current as the $NaNO_2$ concentration increases. The measured current over time with different $NaNO_2$ concentrations by chronoamperometry appears in Figure S6. In the 10 mM $NaNO_2$ solution, the electrolysis current is greater at the reduction peak voltage (−1.84 V) which is consistent with the CV results.

The electrolytic production of NO by the biodegradable battery module consisting of 4 Zn−Mo cells in series is evaluated as a function of time in Tyrode's solution with $NaNO_2$ (10 mM), and the results are shown in Figure 5d. The measured output voltage provided by the battery module during electrolysis is approximately −1.8 − −2.0 V. 3-Amino-4-(*N*-methylamino)-2′,7′-difluorofluorescein (DAF-FM), one of the most sensitive fluorescence probes for capturing NO proposed in recent years,[50] is used as the quantification agent, and the corresponding calibration curve appears in Figure S7a. The results indicate that the power offered by the biodegradable Zn−Mo battery module successfully enables the generation of NO (100−300 μM) and that the amount of detected NO increases with time (Figure 5d). Electrolytic NO production with various voltages (−1.6, −1.8, and −2.0 V) applied by a potentiostat is also performed (Figure S7b), and the amount of generated NO increases monotonically with the electrolysis time (200, 400, and 600 s). Given the similar applied voltage, the amount of NO generated by the biodegradable battery module is comparable to that by the potentiostat. These results suggest that the electrochemical generation of NO can be modulated by applied voltage and electrolysis time. The Faraday efficiency of NO production (FE^{NO}) is calculated to be from 7 to 20% and increases with the electrolysis time (Figure S7c).

Electrochemical NO generation with power sources provided by the biodegradable Zn−Mo battery module is then performed to modulate the activities of the HEK 293T cells. HEK cells are immersed in Tyrode's solution containing 0 or 10 mM $NaNO_2$. In the first 300 s, the fluorescence intensity remains unchanged in the absence of an electric field, which serves as the baseline for subsequent experiments (Figure 5e). At 300 s, a voltage is supplied to the solution by a potentiostat (−1.6 V) (Figure 5e(i,iii)) or a Zn−Mo battery module (Figure 5e(ii,iv)) to trigger the electrolytic generation of NO. A significant change in fluorescence intensity is observed within 400−500 s in the solution with 10 mM $NaNO_2$ (Figure 5e(iii,iv)), while the fluorescence intensity remains unchanged without $NaNO_2$ regardless of whether a voltage is applied (Figure 5e(i,ii))). The output voltage of the battery module is measured to be approximately −1.7 V during the electrolysis with HEK cells. Representative fluorescent intensity changes in HEK cells triggered by NO generation driven by Zn−Mo batteries appear in Figure S8. The maximum fluorescence intensity of each cell is quantified, and the statistical results are given in Figure 5f. These results confirm that the biodegradable Zn−Mo batteries accomplish power

https://doi.org/10.1021/acsnano.2c12125
ACS Nano 2023, 17, 5727−5739

supply for electrochemical NO production capable of modulating the behavior of cellular network, with efficacy comparable to that with power offered by an external potentiostat. The proposed Zn−Mo primary battery system can therefore enable an innovative and fully degradable electronic medicine platform for controlled NO delivery, providing timely and accurate treatments of NO associated diseases, which could be beneficial to regulate disorders or injuries of the nervous system at the cellular level.[61,62] As NO has essential roles in regulating vasodilation, facilitating spinal cord repair, and offering chemical pathways for neuromodulation, the development of electrochemical generation of NO based on fully degradable biobatteries could therefore offer an alternative route that benefits future medical treatments.

Finally, to evaluate the biocompatibility and biodegradability, the biodegradable Zn−Mo battery module (4 Zn−Mo cells in series) is encapsulated with PLGA and implanted into the subcutaneous area of the posterior back of SD rats. As shown in Figure 6a, 2 weeks after implantation, swelling is observed at the implantation site, which is speculated to be related to the swelling and deformation of the battery constituent materials and the immune response associated with implantation surgeries. Hematology and blood chemistry analyses at 2 weeks postoperatively show minimal differences compared with the control group (Figure S9), indicating no sign of significant adverse effects associated with battery implantation. At 12 weeks postoperatively, the battery module completely degrades, and subcutaneous tissues at the implantation sites remain in healthy status (Figure 6a). The degradation process of the battery module is tracked by micro-CT, and the results at 4, 6, 8, and 12 weeks are shown in Figure 6b. After 4 weeks of implantation, micro-CT images show the battery in a round shape with an inner holler cavity, probably due to the continuous swelling of polymeric components during hydrolysis. The remaining battery components gradually decrease in size over time and almost disappear altogether after 12 weeks, indicating the degradability of Zn−Mo battery module *in vivo*. Hematoxylin and eosin (H&E) images of the tissues at the implantation sites appear in Figure 6c, and results at 12 weeks postoperatively are comparable with those of the control group, indicating desirable biocompatibility and the complete biodegradation of Zn−Mo batteries. The blood analysis and H&E images of major organs in different stages are shown in Figures S9 and S10, respectively. No significant inflammatory response is observed.

CONCLUSION

In this work, we propose a fully biodegradable primary Zn−Mo battery with anode electrodes based on sintered nanoparticles and normal saline or gelatin hydrogel serves as the electrolyte. The battery has the advantages of full degradation, prolonged operational lifetime (up to ∼19 days) and desirable output voltage (up to ∼0.7 V) and energy capacity (>1500 μWh) compared with reported primary Zn biobatteries. The constituent materials of Zn−Mo batteries demonstrate excellent biocompatibility and biodegradability both *in vitro* and *in vivo*. The biodegradable Zn−Mo batteries are shown to promote the proliferation of Schwann cells and the axonal growth of DRG. By the introduction of gelatin electrolyte and putting 4 Zn−Mo cells in series, a fully biodegradable battery module is achieved with a promoted voltage up to 2.3 V. The biodegradable battery module successfully works as the power source for electrochemical NO generation and can modulate the behavior of cellular network, with efficacy comparable to conventional power supply.

The materials strategies and fabrication schemes proposed in this work lay the foundation for the development of fully bioresorbable power devices and could enable innovative, biodegradable, and self-powered electronic medicine. Future interesting directions include the exploration of biodegradable primary batteries with voltage and operation time frames in a wider range, fully implantable platform to achieve self-powered drug delivery, the incorporation of intelligent switches to realize on-demand electric field, the integration of multiple drug sources capable of electrolytic production, *etc*. The advancement of biodegradable power devices for electronic medicine could have great potential in putting forward emerging disease treatments and fulfilling unmet clinical needs.

METHODS

Fabrication of Zn−Mo Primary Batteries. Zn powders with a particle size of 50 nm (Deco Island Gold, China) were mixed with isopropyl alcohol (IPA) with a ratio of 1 g/3 mL by a magnetic stirrer (IKA, Germany) at room temperature to achieve Zn slurries. Mo powders with a particle size of 2 μm (Deke Island Gold, China) were cleaned 3 times with diluted hydrochloric acid (10%) and anhydrous ethanol to remove surface oxides. Mo powders, PLGA, and acetone were mixed with the ratio of 6 g/1 g/10 mL to achieve Mo slurries. To evaluate the characteristic of battery electrodes, Pt foils were encapsulated with epoxy resin, exposing an area of 1 cm^2 as the current collector. The Zn slurry (100 μL) was slowly drop-cast on the exposed area of Pt foils, and the acetic acid solution (10%) was then uniformly added onto the surface of Zn slurries. Electrochemical sintering was carried out at room temperature, and the remaining acetic acid is completely dried out to achieve the Zn electrodes. Twenty microliters of PLGA in acetone (PLGA/acetone = 1 g/10 mL) was added to the surface of the Zn electrode as a thin encapsulation layer to stabilize the sintered structure. Similarly, the Mo slurry was drop-cast onto the exposed surface of Pt foils to achieve Mo electrodes. A biodegradable battery module with multiple Zn−Mo cells in series was achieved by the process method shown in Figure 4a. Fifty microliter Mo slurries were drop-cast on the surface of polytetrafluoroethylene (PTFE) mold to realize Mo electrodes (0.5 cm × 0.7 cm). A 10% PLGA/acetone solution was drop-cast on top of the Mo electrode with an area of 0.5 cm × 1.2 cm. Then the two-layer thin film was removed from the PTFE mold, and 40 μL of Zn slurries (0.5 cm × 0.5 cm) was drop-cast on the PLGA surface without the Mo electrode. With the diffusion and volatilization of IPA, a small amount of Zn powder entered the region of the Mo electrode, forming an overlapping area with a width of 1 mm to achieve a connection between different cells. Acetic acid was applied to realize sintering and complete the formation of the Zn electrodes. Gelatin with NaCl (9 wt %) served as the electrolyte for the battery module. The gel electrolyte was obtained by mixing sodium chloride (NaCl) and gelatin particles with deionized water with the ratio of 0.9 g/1 g/10 mL through stirring at 40 °C for 1 h, followed by cooling and shaping in molds with a size of 2 cm × 2 cm × 0.5 cm. The gel electrolyte was then cut into small pieces (0.5 × 0.5 cm) and assemble with the individual Zn−Mo battery (0.5 cm × 0.5 cm) in a sandwich structure to achieve the serial connection of multiple Zn−Mo cells.

Materials and Characterization of Zn−Mo Batteries. Zn electrodes before and after room temperature sintering are observed under an SEM (Zeiss GEMINISEM 500, Germany). A potentiostat (Gamry, USA) was used to conduct EIS tests on Zn and Mo electrodes based on foils and particles and evaluate the differences in charge transfer resistance. The EIS tests were conducted with a three-electrode configuration. Normal saline (0.9 wt % NaCl, pH 7, Leagene Biotechnology, China), PBS (pH 7.4, Solarbio, China), or gastric juice (pH 2, Leagene Biotechnology, China) was used as the

https://doi.org/10.1021/acsnano.2c12125
ACS Nano 2023, 17, 5727−5739

electrolyte, with silver/silver chloride (Ag/AgCl) and Pt as the reference and counter electrodes, respectively. The scan frequency ranged from 0.1 to 10,000 Hz. The electrode area was 1 cm^2, and the foil electrodes were polished with sandpaper to obtain a smooth surface before the measurement. The evaluation of battery performance was carried out in a beaker with two electrodes immersed in the electrolyte to assemble a primary battery with an electrode spacing of 2 cm. A multichannel battery test system (Neware, Shenzhen China) was used to investigate the discharge behavior as a function of time, type of electrolyte, and current densities. The discharge behavior of the battery module with 2, 4, and 6 Zn−Mo cells in series was also tested, with a discharge current of 10 μA, corresponding to a current density of 40 $\mu A/cm^2$. The mechanical properties of Mo and Zn electrodes were measured by micro-in situ mechanical experimental system (CARE Test IBTC-300SL, Tianjin) with a strain rate of 1%/s.

***In Vitro* Studies with Schwann Cells.** Schwann cells were obtained as described previously[63] and were cultured with the extract solutions of Zn and Mo electrodes to evaluate cytocompatibility. Detailed procedure is as follows: Zn and Mo slurries (1 μL) were drop-cast, respectively, on top of the cell climbing sheets of the 24-well plates to achieve Zn and Mo electrodes. PLGA/acetone solution (10 μL) was added on top of the metallic electrodes as an encapsulation. According to the standard ISO-10993, the ratio of sample surface area to the volume of the medium of 1.24 cm^2 mL^{-1} was realized by covering 1.54 cm^2 electrode surface with 1.25 mL of Schwann cell culture medium (DMEM/F12 (Gibco, USA), 10% FBS, 2 mmol L^{-1} GLUTamax-1, 1× cynostreptomycin double antibody, 2 μM phloressin, 10 ng ML-1 EGF-D). After soaking for 1 and 3 days, the extracts of Zn and Mo electrodes were collected and stored at 4 °C in the refrigerator. Schwann cells were seeded in 96-well plates with a density of 3000 cells per well and placed in an incubator for 6 h. The culture medium was then replaced with the extracts of Zn and Mo electrodes and cultured for 3 days. A CCK-8 kit was used to quantify cell proliferation. Zn−Mo batteries are also cocultured with Schwann cells to study the potential influence of electric field. 1 μLof Zn and Mo slurries was drop-cast onto the surface of cell climbing sheets with a spacing of 8 mm, followed by the addition of 10 μL of PLGA/acetone solution as an encapsulation. Schwann cells were then seeded into 24-well plates with Zn−Mo batteries at a density of 6000 cells per well and incubated for 1, 3, and 7 days, respectively. Cell proliferation was detected using the CCK-8 kit.

***In Vitro* Studies with DRG.** DRG were obtained from newborn SD rats following a previously reported procedure.[64] Zn and Mo electrodes were cocultured with DRG to explore biocompatibility and the effects on axonal growth. Four groups of experiments were performed: control group (without electrode materials), Zn−Mo group (with Zn−Mo batteries), Zn group (only Zn electrodes), and Mo group (only Mo electrodes). The electrodes were achieved on glass culture dishes with a diameter of 6 cm, and 10 μL of PLGA was applied for encapsulation. The electrode spacing was 2 cm. The culture medium consisted mainly of DMEM/F12 (Gibco, USA), plus 2% B-27 (Gibco, USA), and 1% penicillin-streptomycin and was changed every 2 days. After 7 days of culturing, DRG were stained with specific steps as follows: cells were fixed with 4% paraformaldehyde and cleaned 3 times with PBS (5 min for each wash). 0.1% Triton X-100 (China) solution was used for 5 min, followed by PBS cleaning. 10% common goat serum (Solarbio, China) was used for incubation at 37 °C for 30 min. After the goat serum was removed, mouse anti-NF200 antibody (Sigma-Aldrich, USA) and rabbit anti-S100 antibody (Sigma-Aldrich, USA) were added and incubated overnight at 4 °C. Goat anti-rabbit antibody (IgG H+L, Alexa Fluor 594, Abcam, USA) and goat anti-mouse antibody (IgG H+L, Alexa Fluor 488, Abcam, USA) were added and incubated at room temperature in dark conditions for 1 h, followed by washing with PBS 3 times. 4′, 6-Diamidine-2-phenylindole dye (4′,6-diamidino-2-phenylindole, DAPI) was added under dark conditions to stain the nucleus for 5 min, followed by cleaning with PBS three times. Cells were observed by confocal laser microscopy (LSM780, Zeiss, Oberkochen, Germany). The axonal growth of DRG was statistically analyzed using ImageJ software (Wayne Rasband National Institutes of Health, USA).

NO Calibration Curves. In order to quantify the concentration of NO generated through electrolysis, the diamino fluorescein derivative DAF-FM was used as the fluorescent probe. DEA NONOate was used as the NO donor to establish a calibration curve. The equivalent ratio of DEA NONOate to NO was 1.5:1. Tyrode's solution (Leagene Biotechnology, China) with different concentrations of DEA NONOate (300, 150, 75, 37.5, and 18.75 μM) was prepared. Fluorescence probe DAF-FM was dissolved in dimethyl sulfoxide (DMSO) at a concentration of 300 μM. DEA NONOate solutions (100 μL) and DAF-FM solution (100 μL) were mixed in 96-well plates, followed by standing for 20 min at room temperature. The absorbance value of the mixed solution in 96-well plates was measured by a microplate reader (PerkinElmer, USA), with the emission wavelength of 495 nm and the absorption wavelength of 515 nm. The standard calibration curve of NO was obtained by linearly fitting the measured fluorescence intensities and concentration of NO.

Electrochemical NO Generation and Analysis. CV and current−time (I−t) curves were first measured with a two-electrode configuration (Pt wires as the counter and reference electrodes) with a CHI650 potentiostat (Chenhua CHI650, China) to obtain suitable electrolysis conditions. The scan rate of the CV was 20 mV/s. In a dark environment, 100 μL of DAF-FM solution and 100 μL of $NaNO_2$ solution were mixed in 96-well plates, and two Pt wire electrodes were used as electrodes with a spacing of 5 mm for electrolytic NO generation. A CHI650 potentiostat and a biodegradable battery module (4 Zn−Mo cells in series) were used to apply voltage for electrolysis. The voltage provided by the potentiostat was −1.6, −1.8, and −2.0 V, and the voltage provided by the battery module was measured to be around −1.8— −2.0 V by a multimeter during the electrolysis process. The fluorescence intensities of sample solutions with electrolysis for 200, 400, and 600 s were measured successively.

Transfection of HEK 293T Cells. The plasmids carrying TRPV1 and the plasmids carrying GCaMP6s were cotransfected into HEK 293T cells by the following steps: HEK 293T cells were placed in 35 mm cell culture dishes to proliferate to a density of ∼70% for later transfection. OPTI-MEM Medium (125 μL) was added to centrifuge tubes (2 tubes, each of 1.5 mL), with Lipo 2000 (4 μL) added in one tube and TRPV1 (1 μg) and GCaMP6s (1 μg) added in the other tube to make a Lipo volume to total plasmid volume ratio of 2:1. The two centrifugal tubes were then shaken for 5 s, centrifuged for 2 s by hand-held centrifuge, and left to stand for 2 min. The opti-MEM medium containing plasmids in one centrifugal tube was then mixed with the other centrifugal tube containing Lipo, pipetted slowly to avoid bubbles, and left still for 3−5 min. All 250 μL of liquid was slowly and evenly added into a 35 mm Petri dish and was placed in a cell culture incubator. After 12 h, the cell status was observed and the medium for normal feeding was replaced. After 48 h, the cells were digested and cultured on a glass coverslip (1 cm in diameter) in a culture dish. Twelve hours later, the adhered cells were used for calcium imaging.

Calcium Imaging of HEK 293T Cells upon Electrolytic NO Generation. The glass covered with transfected HEK 293T cells was placed in a 35 mm Petri dish containing 2 mL of Tyrode's solution. The fluorescence intensity changes in HEK 293T cells were observed with an inverted fluorescence microscope and recorded by a micro-Manager software at an interval of 5 s. The exposure time is 33 μs (excitation wavelength at 488 nm, emission wavelength at 507 nm). HEK 293T cells were stimulated by DEA NONOate (a NO donor).

In the case of testing transfection efficacy, 100 μL of 10 mM DEA NONOate solution was added into the Petri dish through a microperfusion device three hundred seconds after the experiment started, and the change of cell fluorescence intensity was observed. In the case of testing electrochemical NO production, the response of HEK 293T cells upon the generation of NO driven by a potentiostat (−1.6 V, CHI650) or a Zn−Mo battery module were measured, with different $NaNO_2$ concentrations in Tyrode's solution (0 or 10 mM). Two Pt electrodes were fixed near the glass coverslip in the same Petri

https://doi.org/10.1021/acsnano.2c12125
ACS Nano 2023, 17, 5727−5739

dish. After 300 s, voltage was supplied and lasted for 150 s. During the electrolysis process, a multimeter was used to monitor the output voltage of the battery module. ImageJ software was used to analyze the changes of the fluorescence intensity of each cell over time. Three batches of experiments were performed for each condition.

***In Vivo* Evaluation of Biodegradation and Biocompatibility.** The *in vivo* degradation of the Zn−Mo battery module with PLGA encapsulation was investigated by using SD rats. Animal procedures were performed in agreement with the institutional guidelines of Tsinghua University. Protocols were reviewed and approved by the Institutional Animal Care and Use Committee (IACUC) at Tsinghua University. With isoflurane gas anesthesia, the back skin of the anesthetized animal was open and the battery module was implanted at the exposed subcutaneous tissue and sutured. Micro-CT was used to track the degradation process at various stages. Blood samples from the tails of SD rats were collected for hematology and blood chemistry analysis. HE staining analysis were performed on the surrounding tissues at the implantation sites 12 weeks postoperatively.

Statistical Data Analysis. Data are shown by mean ± standard deviation. SPSS (IBM, USA) and PrismPad software were used for analysis of variance (ANOVA) and independent *t* test analysis. $^{*}P < 0.05$ was considered as significant difference, with $^{**}P < 0.01$, $^{***}P < 0.001$, with "ns" representing no statistical difference.

ASSOCIATED CONTENT

Data Availability Statement

All data needed to evaluate the conclusions in the paper are present in the paper and/or the Supporting Information.

Supporting Information

The Supporting Information is available free of charge at https://pubs.acs.org/doi/10.1021/acsnano.2c12125.

Electrochemical impedance spectroscopy characteristics of electrodes based on foils and metallic particles in gastric juice (pH 2), phosphate-buffered saline (pH 7.4) and normal saline (pH 7); discharge behavior of Zn−Mo batteries with foil and particle electrodes in gastric juice (pH 2), phosphate-buffered saline (pH 7.4) and normal saline (pH 7); mechanical properties of Zn−Mo battery materials; influence of Zn and Mo electrodes on proliferation of Schwann cells and the growth behavior of DRG; CV curves with different concentrations of $NaNO_2$ in Tyrode's solution; *I*−*t* curves of NO generation with different concentrations of $NaNO_2$ in Tyrode's solution; characteristics of the electrochemical generation of NO; representative fluorescent intensity changes in HEK cells triggered by NO generation driven by Zn−Mo batteries; hematology and blood chemistry analysis of SD rats implanted with Zn−Mo batteries (experimental group) and the control group; hematoxylin and eosin staining images of major organs of SD rats (heart, liver, spleen, lungs, and kidneys) at different stages after the implantation of the Zn−Mo battery module; comparison of reported primary Zn biobatteries; mechanical properties of electrodes, PLGA and gelatin electrolyte (PDF)

AUTHOR INFORMATION

Corresponding Authors

Lan Yin − *School of Materials Science and Engineering, The Key Laboratory of Advanced Materials of Ministry of Education, State Key Laboratory of New Ceramics and Fine Processing, , Center for Flexible Electronics Technology, Tsinghua University, Beijing 100084, China;* orcid.org/0000-0001-7306-4628; Email: lanyin@tsinghua.edu.cn

Wei Xiong − *School of Life Sciences, IDG/McGovern Institute for Brain Research, Tsinghua University, Beijing 100084, China;* Present Address: Chinese Institute for Brain Research, Beijing, 102206, China; Email: wei_xiong@cibr.ac.cn

Authors

Xueying Huang − *School of Materials Science and Engineering, The Key Laboratory of Advanced Materials of Ministry of Education, State Key Laboratory of New Ceramics and Fine Processing, , Center for Flexible Electronics Technology, Tsinghua University, Beijing 100084, China*

Hanqing Hou − *School of Life Sciences, IDG/McGovern Institute for Brain Research, Tsinghua University, Beijing 100084, China*

Bingbing Yu − *School of Materials Science and Engineering, The Key Laboratory of Advanced Materials of Ministry of Education, State Key Laboratory of New Ceramics and Fine Processing, , Center for Flexible Electronics Technology, Tsinghua University, Beijing 100084, China*

Jun Bai − *Institute of Orthopedics, Chinese PLA General Hospital, Beijing 100853, China*

Yanjun Guan − *Institute of Orthopedics, Chinese PLA General Hospital, Beijing 100853, China*

Liu Wang − *Key Laboratory of Biomechanics and Mechanobiology of Ministry of Education, Beijing Advanced Innovation Center for Biomedical Engineering, School of Biological Science and Medical Engineering, and with the School of Engineering Medicine, Beihang University, Beijing 100083, China*

Kuntao Chen − *School of Materials Science and Engineering, The Key Laboratory of Advanced Materials of Ministry of Education, State Key Laboratory of New Ceramics and Fine Processing, , Center for Flexible Electronics Technology, Tsinghua University, Beijing 100084, China*

Xibo Wang − *School of Materials Science and Engineering, The Key Laboratory of Advanced Materials of Ministry of Education, State Key Laboratory of New Ceramics and Fine Processing, , Center for Flexible Electronics Technology, Tsinghua University, Beijing 100084, China*

Pengcheng Sun − *School of Materials Science and Engineering, The Key Laboratory of Advanced Materials of Ministry of Education, State Key Laboratory of New Ceramics and Fine Processing, , Center for Flexible Electronics Technology, Tsinghua University, Beijing 100084, China*

Yuping Deng − *School of Materials Science and Engineering, The Key Laboratory of Advanced Materials of Ministry of Education, State Key Laboratory of New Ceramics and Fine Processing, , Center for Flexible Electronics Technology, Tsinghua University, Beijing 100084, China*

Shangbin Liu − *School of Materials Science and Engineering, The Key Laboratory of Advanced Materials of Ministry of Education, State Key Laboratory of New Ceramics and Fine Processing, , Center for Flexible Electronics Technology, Tsinghua University, Beijing 100084, China*

Xue Cai − *Department of Electronic Engineering, Beijing National Research Center for Information Science and Technology, Institute for Precision Medicine, Center for Flexible Electronics Technology, and IDG/McGovern Institute for Brain Research, Tsinghua University, Beijing 100084, China*

Yu Wang − *Institute of Orthopedics, Chinese PLA General Hospital, Beijing 100853, China*

https://doi.org/10.1021/acsnano.2c12125
ACS Nano 2023, 17, 5727−5739

Jiang Peng − *Institute of Orthopedics, Chinese PLA General Hospital, Beijing 100853, China;* orcid.org/0000-0003-4662-9288

Xing Sheng − *Department of Electronic Engineering, Beijing National Research Center for Information Science and Technology, Institute for Precision Medicine, Center for Flexible Electronics Technology, and IDG/McGovern Institute for Brain Research, Tsinghua University, Beijing 100084, China;* orcid.org/0000-0002-8744-1700

Complete contact information is available at: https://pubs.acs.org/10.1021/acsnano.2c12125

Author Contributions

X.H. and L.Y. conceived and designed the research project. X.H., B.Y., Y.D., and L.Y. designed and fabricated the devices. X.H., B.Y., and L.Y. performed data analysis. X.H., H.H., B.Y., Y.G., J.B., P.S., and L.Y. performed the cell toxicity tests and data analysis. X.H., H.H., B.Y., and L.Y. performed the animal studies. X.H., H.H., B.Y., K.C., W.X., and L.Y. designed and performed cell transfection and electrolysis stimulation. S.L. contributed to the photographs and schematic diagrams in the manuscript. X.H., W.X., and L.Y. wrote the manuscript with input from all authors. X.H., H.H., and B.Y. contributed equally to the paper.

Notes

The authors declare no competing financial interest.

ACKNOWLEDGMENTS

The project was supported by the National Natural Science Foundation of China (52171239, T2122010 to L.Y, 52272277 to X.S.), and Tsinghua University-Peking Union Medical College Hospital Initiative Scientific Research Program (20191080592).

REFERENCES

(1) Choi, Y. S.; Yin, R. T.; Pfenniger, A.; Koo, J.; Avila, R.; Benjamin Lee, K.; Chen, S. W.; Lee, G.; Li, G.; Qiao, Y.; Murillo-Berlioz, A.; Kiss, A.; Han, S.; Lee, S. M.; Li, C.; Xie, Z.; Chen, Y.-Y.; Burrell, A.; Geist, B.; Jeong, H.; et al. Fully Implantable and Bioresorbable Cardiac Pacemakers without Leads or Batteries. *Nat. Biotechnol.* **2021**, *39*, 1228−1238.

(2) Koo, J.; MacEwan, M. R.; Kang, S.-K.; Won, S. M.; Stephen, M.; Gamble, P.; Xie, Z.; Yan, Y.; Chen, Y.-Y.; Shin, J.; Birenbaum, N.; Chung, S.; Kim, S. B.; Khalifeh, J.; Harburg, D. V.; Bean, K.; Paskett, M.; Kim, J.; Zohny, Z. S.; Lee, S. M.; et al. Wireless Bioresorbable Electronic System Enables Sustained Nonpharmacological Neuroregenerative Therapy. *Nat. Med.* **2018**, *24*, 1830−1836.

(3) Choi, Y. S.; Hsueh, Y.-Y.; Koo, J.; Yang, Q.; Avila, R.; Hu, B.; Xie, Z.; Lee, G.; Ning, Z.; Liu, C.; Xu, Y.; Lee, Y. J.; Zhao, W.; Fang, J.; Deng, Y.; Lee, S. M.; Vázquez-Guardado, A.; Stepien, I.; Yan, Y.; Song, J. W.; et al. Stretchable, Dynamic Covalent Polymers for Soft, Long-Lived Bioresorbable Electronic Stimulators Designed to Facilitate Neuromuscular Regeneration. *Nat. Commun.* **2020**, *11*, 5990.

(4) Wang, L.; Lu, C.; Yang, S.; Sun, P.; Wang, Y.; Guan, Y.; Liu, S.; Cheng, D.; Meng, H.; Wang, Q.; He, J.; Hou, H.; Li, H.; Lu, W.; Zhao, Y.; Wang, J.; Zhu, Y.; Li, Y.; Luo, D.; Li, T.; et al. A Fully Biodegradable and Self-Electrified Device for Neuroregenerative Medicine. *Sci. Adv.* **2020**, *6*, No. eabc6686.

(5) Liu, Y.; Dzidotor, G.; Le, T. T.; Vinikoor, T.; Morgan, K.; Curry, E. J.; Das, R.; McClinton, A.; Eisenberg, E.; Apuzzo, L. N.; Tran, K. T. M.; Prasad, P.; Flanagan, T. J.; Lee, S.-W.; Kan, H.-M.; Chorsi, M. T.; Lo, K. W. H.; Laurencin, C. T.; Nguyen, T. D. Exercise-Induced Piezoelectric Stimulation for Cartilage Regeneration in Rabbits. *Sci. Trans. Med.* **2022**, *14*, No. eabi7282.

(6) Huang, X.; Wang, L.; Wang, H.; Zhang, B.; Wang, X.; Stening, R. Y. Z.; Sheng, X.; Yin, L. Materials Strategies and Device Architectures of Emerging Power Supply Devices for Implantable Bioelectronics. *Small* **2020**, *16*, 1902827.

(7) Yin, L.; Huang, X.; Xu, H.; Zhang, Y.; Lam, J.; Cheng, J.; Rogers, J. A. Materials, Designs, and Operational Characteristics for Fully Biodegradable Primary Batteries. *Adv. Mater.* **2014**, *26*, 3879−84.

(8) Tsang, M.; Armutlulu, A.; Martinez, A. W.; Allen, S. A. B.; Allen, M. G. Biodegradable Magnesium/Iron Batteries with Polycaprolactone Encapsulation: A Microfabricated Power Source for Transient Implantable Devices. *Microsyst. Nanoeng.* **2015**, *1*, 15024.

(9) Nadeau, P.; El-Damak, D.; Glettig, D.; Kong, Y. L.; Mo, S.; Cleveland, C.; Booth, L.; Roxhed, N.; Langer, R.; Chandrakasan, A. P.; Traverso, G. Prolonged Energy Harvesting for Ingestible Devices. *Nat. Biomed. Eng.* **2017**, *1*, 0022.

(10) Huang, X.; Wang, D.; Yuan, Z.; Xie, W.; Wu, Y.; Li, R.; Zhao, Y.; Luo, D.; Cen, L.; Chen, B.; Wu, H.; Xu, H.; Sheng, X.; Zhang, M.; Zhao, L.; Yin, L. A Fully Biodegradable Battery for Self-Powered Transient Implants. *Small* **2018**, *14*, 1800994.

(11) Lee, M. H.; Lee, J.; Jung, S.-K.; Kang, D.; Park, M. S.; Cha, G. D.; Cho, K. W.; Song, J.-H.; Moon, S.; Yun, Y. S.; Kim, S. J.; Lim, Y. W.; Kim, D.-H.; Kang, K. A Biodegradable Secondary Battery and Its Biodegradation Mechanism for Eco-Friendly Energy-Storage Systems. *Adv. Mater.* **2021**, *33*, 2004902.

(12) Kim, Y. J.; Wu, W.; Chun, S. E.; Whitacre, J. F.; Bettinger, C. J. Biologically Derived Melanin Electrodes in Aqueous Sodium-Ion Energy Storage Devices. *Proc. Natl. Acad. Sci. U.S.A.* **2013**, *110*, 20912−7.

(13) Li, H.; Zhao, C.; Wang, X.; Meng, J.; Zou, Y.; Noreen, S.; Zhao, L.; Liu, Z.; Ouyang, H.; Tan, P.; Yu, M.; Fan, Y.; Wang, Z. L.; Li, Z. Fully Bioabsorbable Capacitor As an Energy Storage Unit for Implantable Medical Electronics. *Adv. Sci.* **2019**, *6*, 1801625.

(14) Sheng, H.; Zhou, J.; Li, B.; He, Y.; Zhang, X.; Liang, J.; Zhou, J.; Su, Q.; Xie, E.; Lan, W.; Wang, K.; Yu, C. A Thin, Deformable, High-Performance Supercapacitor Implant That Can Be Biodegraded and Bioabsorbed within an Animal Body. *Sci. Adv.* **2021**, *7*, No. eabe3097.

(15) Lee, Y.; Bandari, V. K.; Li, Z.; Medina-Sánchez, M.; Maitz, M. F.; Karnaushenko, D.; Tsurkan, M. V.; Karnaushenko, D. D.; Schmidt, O. G. Nano-Biosupercapacitors Enable Autarkic Sensor Operation in Blood. *Nat. Commun.* **2021**, *12*, 4967.

(16) Koo, J.; MacEwan, M. R.; Kang, S. K.; Won, S. M.; Stephen, M.; Gamble, P.; Xie, Z. Q.; Yan, Y.; Chen, Y. Y.; Shin, J.; Birenbaum, N.; Chung, S. J.; Kim, S. B.; Khalifeh, J.; Harburg, D. V.; Bean, K.; Paskett, M.; Kim, J.; Zohny, Z. S.; Lee, S. M.; et al. Wireless Bioresorbable Electronic System Enables Sustained Nonpharmacological Neuroregenerative Therapy. *Nat. Med.* **2018**, *24*, 1830−1836.

(17) Kang, S. K.; Park, G.; Kim, K.; Hwang, S. W.; Cheng, H. Y.; Shin, J. H.; Chung, S. J.; Kim, M.; Yin, L.; Lee, J. C.; Lee, K. M.; Rogers, J. A. Dissolution Chemistry and Biocompatibility of Silicon- and Germanium-Based Semiconductors for Transient Electronics. *ACS Appl. Mater. Interfaces* **2015**, *7*, 9297−9305.

(18) Lu, L. Y.; Yang, Z. J.; Meacham, K.; Cvetkovic, C.; Corbin, E. A.; Vazquez-Guardado, A.; Xue, M. T.; Yin, L.; Boroumand, J.; Pakeltis, G.; Sang, T.; Yu, K. J.; Chanda, D.; Bashir, R.; Gereau, R. W.; Sheng, X.; Rogers, J. A. Biodegradable Monocrystalline Silicon Photovoltaic Microcells As Power Supplies for Transient Biomedical Implants. *Adv. Energy Mater.* **2018**, *8*, 1703035.

(19) Yao, G.; Kang, L.; Li, C.; Chen, S.; Wang, Q.; Yang, J.; Long, Y.; Li, J.; Zhao, K.; Xu, W.; Cai, W.; Lin, Y.; Wang, X. A Self-Powered Implantable and Bioresorbable Electrostimulation Device for Biofeedback Bone Fracture Healing. *Proc. Natl. Acad. Sci. U.S.A.* **2021**, *118*, e2100772118.

(20) Li, Z.; Zhu, G. A.; Yang, R. S.; Wang, A. C.; Wang, Z. L. Muscle-Driven in Vivo Nanogenerator. *Adv. Mater.* **2010**, *22*, 2534−2537.

(21) Bock, D. C.; Marschilok, A. C.; Takeuchi, K. J.; Takeuchi, E. S. Batteries Used to Power Implantable Biomedical Devices. *Electrochim. Acta* **2012**, *84*, 155−164.

(22) Bettucci, O.; Matrone, G. M.; Santoro, F. Conductive Polymer-Based Bioelectronic Platforms toward Sustainable and Biointegrated Devices: A Journey from Skin to Brain across Human Body Interfaces. *Adv. Mater. Technol.* **2022**, *7*, 2100293.
(23) Xia, J.; Yuan, Z.; Cai, F. Toward a Biocompatible and Degradable Battery Using a Mg-Zn-Zr Alloy with B-Tricalcium Phosphate Nanocoating As Anode. *J. Mater. Eng. Perform.* **2018**, *27*, 4005−4009.
(24) Edupuganti, V.; Solanki, R. Fabrication, Characterization, and Modeling of a Biodegradable Battery for Transient Electronics. *J. Power Sources* **2016**, *336*, 447−454.
(25) Jia, X.; Yang, Y.; Wang, C.; Zhao, C.; Vijayaraghavan, R.; MacFarlane, D. R.; Forsyth, M.; Wallace, G. G. Biocompatible Ionic Liquid-Biopolymer Electrolyte-Enabled Thin and Compact Magnesium-Air Batteries. *ACS Appl. Mater. Interfaces* **2014**, *6*, 21110−7.
(26) Tsang, M.; Armutlulu, A.; Herrault, F.; Shafer, R. H.; Allen, S. A. B.; Allen, M. G. Development of Electroplated Magnesium Microstructures for Biodegradable Devices and Energy Sources. *J. Microelectromech. Syst.* **2014**, *23*, 1281−1289.
(27) Song, M.; Tan, H.; Chao, D.; Fan, H. J. Recent Advances in Zn-Ion Batteries. *Adv. Funct. Mater.* **2018**, *28*, 1802564.
(28) Zhang, Y.; Han, X.; Liu, R.; Yang, Z.; Zhang, S.; Zhang, Y.; Wang, H.; Cao, Y.; Chen, A.; Sun, J. Manipulating the Zinc Deposition Behavior in Hexagonal Patterns at the Preferential Zn (100) Crystal Plane to Construct Surficial Dendrite-Free Zinc Metal Anode. *Small* **2022**, *18*, 2105978.
(29) Tian, W.; Li, Y.; Zhou, J.; Wang, T.; Zhang, R.; Cao, J.; Luo, M.; Li, N.; Zhang, N.; Gong, H.; Zhang, J.; Xie, L.; Kong, B. Implantable and Biodegradable Micro-Supercapacitor Based on a Superassembled Three-Dimensional Network Zn@Ppy Hybrid Electrode. *ACS Appl. Mater. Interfaces* **2021**, *13*, 8285−8293.
(30) Swardfager, W.; Herrmann, N.; Mazereeuw, G.; Goldberger, K.; Harimoto, T.; Lanctôt, K. L. Zinc in Depression: A Meta-Analysis. *Bio. Psych.* **2013**, *74*, 872−878.
(31) Institute of Medicine. *Dietary Reference Intakes for Vitamin a, Vitamin K, Arsenic, Boron, Chromium, Copper, Iodine, Iron, Manganese, Molybdenum, Nickel, Silicon, Vanadium, and Zinc*; National Academies Press: Washington, DC, 2001.
(32) Dong, Y.; Li, J.; Yang, F.; Wang, Y.; Zhang, Z.; Wang, J.; Long, Y.; Wang, X. Bioresorbable Primary Battery Anodes Built on Core-Double-Shell Zinc Microparticle Networks. *ACS Appl. Mater. Interfaces* **2021**, *13*, 14275−14282.
(33) Xu, R.; Zhou, J.; Gong, H.; Qiao, L.; Li, Y.; Li, D.; Gao, M.; Xu, G.; Wang, M.; Liang, X.; Zhang, X.; Luo, M.; Qiu, H.; Liang, K.; Li, Y. Environment-Friendly Degradable Zinc-Ion Battery Based on Guar Gum-Cellulose Aerogel Electrolyte. *Biomater. Sci.* **2022**, *10*, 1476−1485.
(34) Jimbo, H.; Miki, N. Gastric-Fluid-Utilizing Micro Battery for Micro Medical Devices. *Sensors Actuators B: Chem.* **2008**, *134*, 219−224.
(35) Zhou, J.; Li, Y.; Xie, L.; Xu, R.; Zhang, R.; Gao, M.; Tian, W.; Li, D.; Qiao, L.; Wang, T.; Cao, J.; Wang, D.; Hou, Y.; Fu, W.; Yang, B.; Zeng, J.; Chen, P.; Liang, K.; Kong, B. Humidity-Sensitive, Shape-Controllable, and Transient Zinc-Ion Batteries Based on Plasticizing Gelatin-Silk Protein Electrolytes. *Mater. Today Energy* **2021**, *21*, 100712.
(36) Zhou, J.; Zhang, R.; Xu, R.; Li, Y.; Tian, W.; Gao, M.; Wang, M.; Li, D.; Liang, X.; Xie, L.; Liang, K.; Chen, P.; Kong, B. Super-Assembled Hierarchical Cellulose Aerogel-Gelatin Solid Electrolyte for Implantable and Biodegradable Zinc Ion Battery. *Adv. Funct. Mater.* **2022**, *32*, 2111406.
(37) Mostafalu, P.; Sonkusale, S. Flexible and Transparent Gastric Battery: Energy Harvesting from Gastric Acid for Endoscopy Application. *Biosens. Bioelectron.* **2014**, *54*, 292−296.
(38) Yin, L.; Cheng, H.; Mao, S.; Haasch, R.; Liu, Y.; Xie, X.; Hwang, S.-W.; Jain, H.; Kang, S.-K.; Su, Y.; Li, R.; Huang, Y.; Rogers, J. A. Dissolvable Metals for Transient Electronics. *Adv. Funct. Mater.* **2014**, *24*, 645−658.
(39) Petrova, M.; Bojinov, M.; Zanna, S.; Marcus, P. Mechanism of Anodic Oxidation of Molybdenum in Nearly-Neutral Electrolytes Studied by Electrochemical Impedance Spectroscopy and X-Ray Photoelectron Spectroscopy. *Electrochim. Acta* **2011**, *56*, 7899−7906.
(40) Chen, Y.; Schneider, P.; Erbe, A. Investigation of Native Oxide Growth on Zinc in Different Atmospheres by Spectroscopic Ellipsometry. *Phys. Status Solidi A* **2012**, *209*, 846−853.
(41) Lee, Y. K.; Kim, J.; Kim, Y.; Kwak, J. W.; Yoon, Y.; Rogers, J. A. Room Temperature Electrochemical Sintering of Zn Microparticles and Its Use in Printable Conducting Inks for Bioresorbable Electronics. *Adv. Mater.* **2017**, *29*, 1702665.
(42) Jayasayee, K.; Clark, S.; King, C.; Dahl, P. I.; Richard Tolchard, J.; Juel, M. Cold Sintering as a Cost-Effective Process to Manufacture Porous Zinc Electrodes for Rechargeable Zinc-Air Batteries. *Processes* **2020**, *8*, 592.
(43) Jia, X.; Wang, C.; Ranganathan, V.; Napier, B.; Yu, C.; Chao, Y.; Forsyth, M.; Omenetto, F. G.; MacFarlane, D. R.; Wallace, G. G. A Biodegradable Thin-Film Magnesium Primary Battery Using Silk Fibroin-Ionic Liquid Polymer Electrolyte. *ACS Energy Lett.* **2017**, *2*, 831−836.
(44) Badawy, W. A.; Al-Kharafi, F. M. Corrosion and Passivation Behaviors of Molybdenum in Aqueous Solutions of Different Ph. *Electrochim. Acta* **1998**, *44*, 693−702.
(45) He, Q.; Huang, Y.; Wang, S. Hofmeister Effect-Assisted One Step Fabrication of Ductile and Strong Gelatin Hydrogels. *Adv. Funct. Mater.* **2018**, *28*, 1705069.
(46) Zuo, K. J.; Gordon, T.; Chan, K. M.; Borschel, G. H. Electrical Stimulation to Enhance Peripheral Nerve Regeneration: Update in Molecular Investigations and Clinical Translation. *Exp. Neurol.* **2020**, *332*, 113397.
(47) Torregrossa, A. C.; Aranke, M.; Bryan, N. S. Nitric Oxide and Geriatrics: Implications in Diagnostics and Treatment of the Elderly. *Proc. Natl. Acad. Sci. U.S.A.* **2011**, *8*, 230−242.
(48) Belzer, V.; Hanani, M. Nitric Oxide As a Messenger between Neurons and Satellite Glial Cells in Dorsal Root Ganglia. *Glia* **2019**, *67*, 1296−1307.
(49) Park, J.; Jin, K.; Sahasrabudhe, A.; Chiang, P. H.; Maalouf, J. H.; Koehler, F.; Rosenfeld, D.; Rao, S.; Tanaka, T.; Khudiyev, T.; Schiffer, Z. J.; Fink, Y.; Yizhar, O.; Manthiram, K.; Anikeeva, P. In Situ Electrochemical Generation of Nitric Oxide for Neuronal Modulation. *Nat. Nanotechnol.* **2020**, *15*, 690−697.
(50) Li, J.; LoBue, A.; Heuser, S. K.; Leo, F.; Cortese-Krott, M. M. Using Diaminofluoresceins (Dafs) in Nitric Oxide Research. *Nitric Oxide* **2021**, *115*, 44−54.
(51) Jiang, Y.; Fu, P.; Liu, Y.; Wang, C.; Zhao, P.; Chu, X.; Jiang, X.; Yang, W.; Wu, Y.; Wang, Y.; Xu, G.; Hu, J.; Bu, W. Near-Infrared Light-Triggered No Release for Spinal Cord Injury Repair. *Sci. Adv.* **2020**, *6*, No. eabc3513.
(52) Caterina, M. J.; Schumacher, M. A.; Tominaga, M.; Rosen, T. A.; Levine, J. D.; Julius, D. The Capsaicin Receptor: A Heat-Activated Ion Channel in the Pain Pathway. *Nature* **1997**, *389*, 816−24.
(53) Caterina, M. J.; Leffler, A.; Malmberg, A. B.; Martin, W. J.; Trafton, J.; Petersen-Zeitz, K. R.; Koltzenburg, M.; Basbaum, A. I.; Julius, D. Impaired Nociception and Pain Sensation in Mice Lacking the Capsaicin Receptor. *Science* **2000**, *288*, 306−313.
(54) Miyamoto, T.; Dubin, A. E.; Petrus, M. J.; Patapoutian, A. Trpv1 and Trpa1Mediate Peripheral Nitric Oxide-Induced Nociception in Mice. *PLoS One* **2009**, *4*, No. e7596.
(55) Calabrese, V.; Mancuso, C.; Calvani, M.; Rizzarelli, E.; Butterfield, D. A.; Giuffrida Stella, A. M. Nitric Oxide in the Central Nervous System: Neuroprotection Versus Neurotoxicity. *Nat. Rev. Neurosci.* **2007**, *8*, 766−775.
(56) Shah, N.; Zhou, L. Regulation of Ion Channel Function by Gas Molecules. *Ion Channels in Biophysics and Physiology* **2021**, *1349*, 139−164.
(57) Simon, J.; Klotz, M. G. Diversity and Evolution of Bioenergetic Systems Involved in Microbial Nitrogen Compound Transformations. *Biochim. Biophys. Acta* **2013**, *1827*, 114−135.

https://doi.org/10.1021/acsnano.2c12125
ACS Nano 2023, 17, 5727−5739

(58) Tocheva, E. I.; Rosell, F. I.; Mauk, A. G.; Murphy, M. E. P. Side-on Copper-Nitrosyl Coordination by Nitrite Reductase. *Science* **2004**, *304*, 867−870.
(59) Einsle, O.; Messerschmidt, A.; Stach, P.; Bourenkov, G. P.; Bartunik, H. D.; Huber, R.; Kroneck, P. M. H. Structure of Cytochrome C Nitrite Reductase. *Nature* **1999**, *400*, 476−480.
(60) Rosca, V.; Duca, M.; de Groot, M. T.; Koper, M. T. M. Nitrogen Cycle Electrocatalysis. *Chem. Rev.* **2009**, *109* (6), 2209−2244.
(61) Nance, E.; Pun, S. H.; Saigal, R.; Sellers, D. L. Drug Delivery to the Central Nervous System. *Nat. Rev. Mater.* **2022**, *7*, 314−331.
(62) Yang, L.; Conley, B. M.; Cerqueira, S. R.; Pongkulapa, T.; Wang, S.; Lee, J. K.; Lee, K.-B. Effective Modulation of Cns Inhibitory Microenvironment Using Bioinspired Hybrid-Nanoscaffold-Based Therapeutic Interventions. *Adv. Mater.* **2020**, *32*, 2002578.
(63) Lu, C.; Wang, Y.; Yang, S.; Wang, C.; Sun, X.; Lu, J.; Yin, H.; Jiang, W.; Meng, H.; Rao, F.; Wang, X.; Peng, J. Bioactive Self-Assembling Peptide Hydrogels Functionalized with Brain-Derived Neurotrophic Factor and Nerve Growth Factor Mimicking Peptides Synergistically Promote Peripheral Nerve Regeneration. *ACS Biomater. Sci. Eng.* **2018**, *4*, 2994−3005.
(64) Gu, Y.; Zhu, J.; Xue, C.; Li, Z.; Ding, F.; Yang, Y.; Gu, X. Chitosan/Silk Fibroin-Based, Schwann Cell-Derived Extracellular Matrix-Modified Scaffolds for Bridging Rat Sciatic Nerve Gaps. *Biomaterials* **2014**, *35*, 2253−2263.

https://doi.org/10.1021/acsnano.2c12125
ACS Nano 2023, 17, 5727−5739

Fully biodegradable and long-term operational primary zinc batteries as power sources for electronic medicine

Authors

Xueying Huang,[1,#] Hanqing Hou,[2,#] Bingbing Yu,[1,#] Jun Bai,[3] Yanjun Guan,[3] Liu Wang,[4] Kuntao Chen,[1] Xibo Wang, [1] Pengcheng Sun,[1] Yuping Deng,[1] Shangbin Liu, [1] Xue Cai, [5] Yu Wang,[3] Jiang Peng,[3] Xing Sheng,[5] Wei Xiong,[2,*] Lan Yin[1,*]

Affiliations

1.X. Huang, B. Yu, K. Chen, X. Wang, P. Sun, Y. Deng, S. Liu, Prof. L. Yin

School of Materials Science and Engineering, The Key Laboratory of Advanced Materials of Ministry of Education, State Key Laboratory of New Ceramics and Fine Processing, Tsinghua University, Center for Flexible Electronics Technology, Beijing, 100084, China

Email: lanyin@tsinghua.edu.cn

2.H. Hou, Prof. W. Xiong

School of Life Sciences, IDG/McGovern Institute for Brain Research, Tsinghua University, Beijing, 100084, China.

Present address: Chinese Institute for Brain Research, Beijing, 102206, China

Email: wei_xiong@cibr.ac.cn

3.J, Bai, Y. Guan, Prof. Y. Wang, Prof. J. Peng

Institute of Orthopedics, Chinese PLA General Hospital, Beijing, 100853, China

4.Prof. L. Wang

Key Laboratory of Biomechanics and Mechanobiology of Ministry of Education, Beijing Advanced Innovation Center for Biomedical Engineering, School of Biological Science and Medical Engineering, and with the School of Engineering Medicine, Beihang University, Beijing 100083, China.

5.X. Cai, Prof. X. Sheng

Department of Electronic Engineering, Beijing National Research Center for Information Science and Technology, Institute for Precision Medicine, Center for Flexible Electronics Technology, and IDG/McGovern Institute for Brain Research, Tsinghua University, Beijing, 100084, China

# Xueying Huang, Hanqing Hou and Bingbing Yu contributed equally to this work

Content

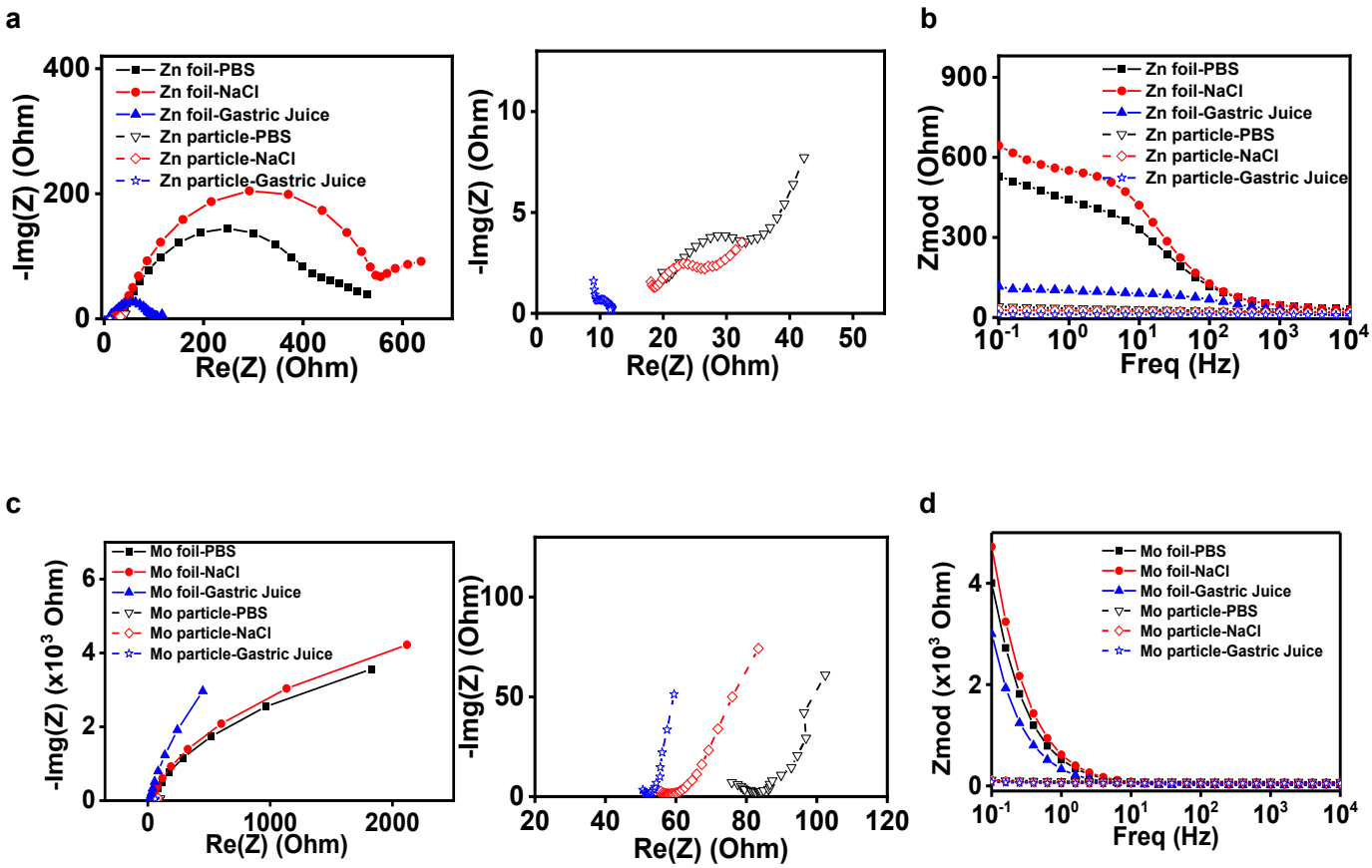

Figure S1. Electrochemical impedance spectroscopy (EIS) characteristics of electrodes based on foils and metallic particles in gastric juice (pH 2), phosphate-buffered saline (PBS, pH 7.4) and normal saline (NaCl, pH 7). a, Nyquist curves of Zn electrodes based on foils and sintered particles in different electrolytes, with enlarged view on the right. **b,** Bode curves of Zn electrodes based on foils and sintered particles in different electrolytes. **c,** Nyquist curves of Mo electrodes based on foils and metallic particles in different electrolytes, with enlarged view on the right. **d,** Bode curves of Mo electrodes based on foils and metallic particles in different electrolytes.

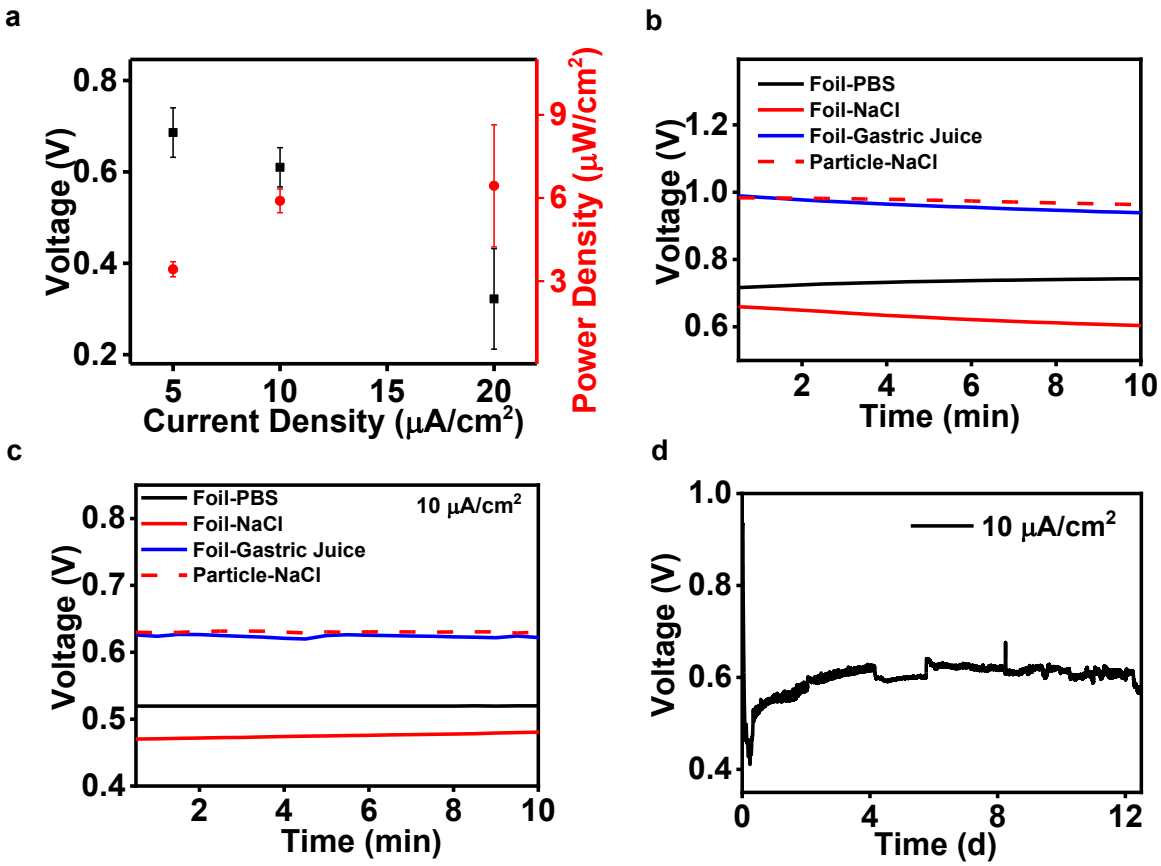

Figure S2. Discharge behavior of Zn-Mo batteries with foil and particle electrodes in gastric juice (pH 2), phosphate-buffered saline (PBS, pH 7.4) and normal saline (NaCl, pH 7). a, Voltage and power density at different discharge current densities. **b,** Open circuit potential of batteries with different electrolytes. **c,** Discharge behavior at 10 μA/cm^2 with different electrolytes. **d,** Long-term discharge behavior of Zn-Mo batteries based on particle electrodes at 10 μA/cm^2.

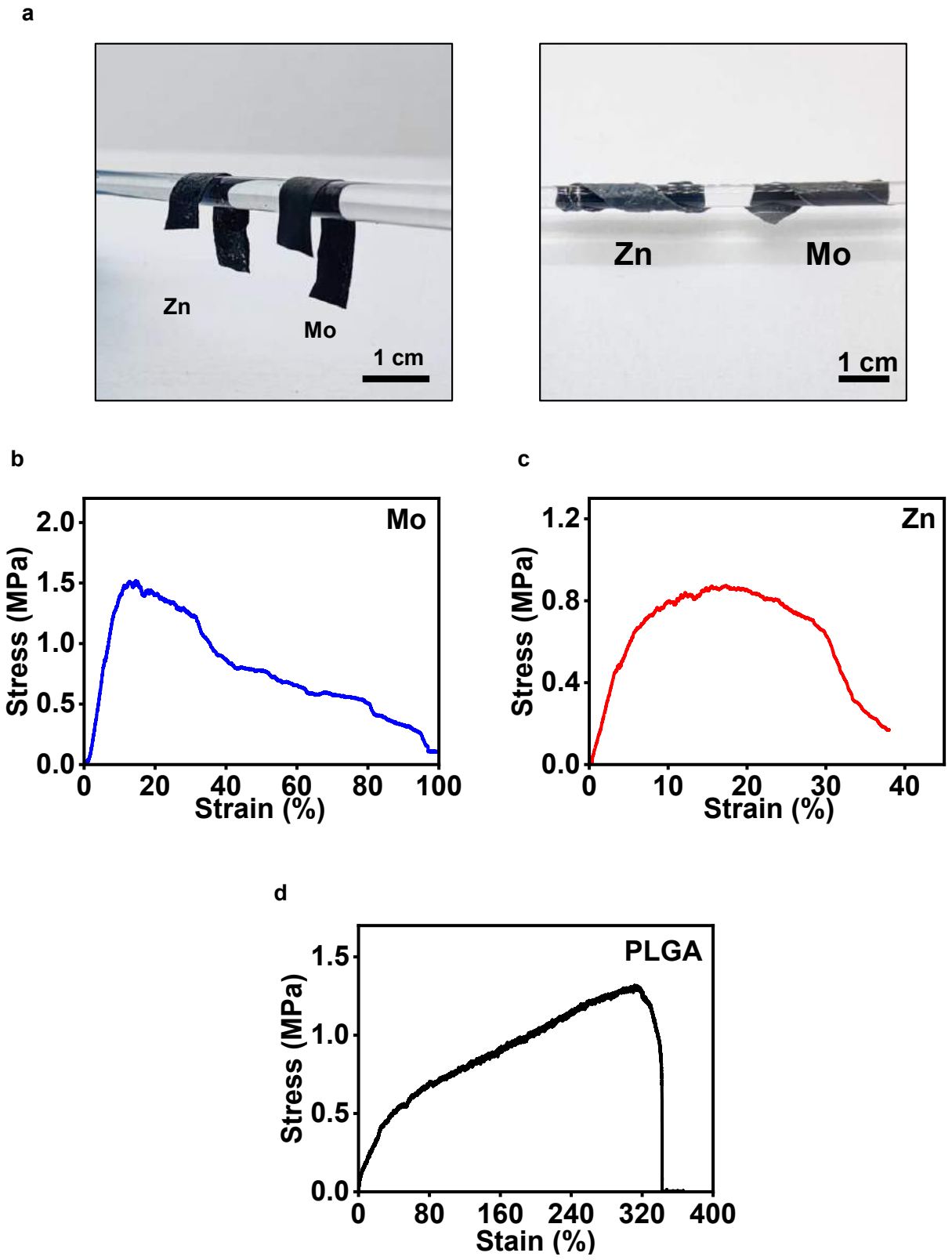

Figure S3. Mechanical properties of Zn-Mo battery materials. a, Photographs of Zn and Mo electrodes demonstrating a certain level of flexibility. **b, c, d,** Mechanical stress-strain curves of Mo electrode, Zn electrode and pure PLGA film, at a strain rate of 1%/s.

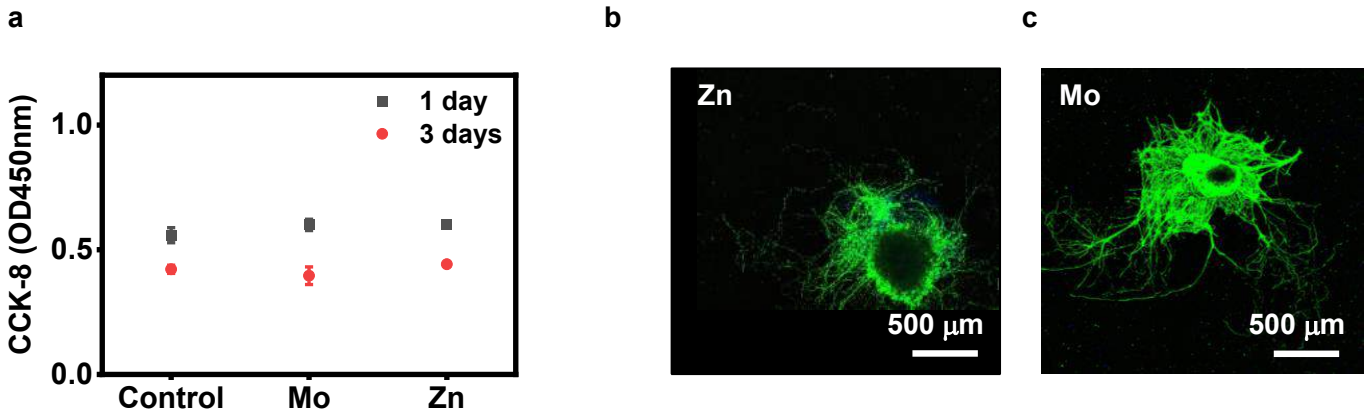

Figure S4. Influence of Zn and Mo electrodes on proliferation of Schwann cells and the growth behavior of DRG. a, Proliferation assay of Schwann cells using the CCK-8 test. **b, c,** Confocal images of the DRG in the Zn and Mo groups. n = 3 independent experiments.

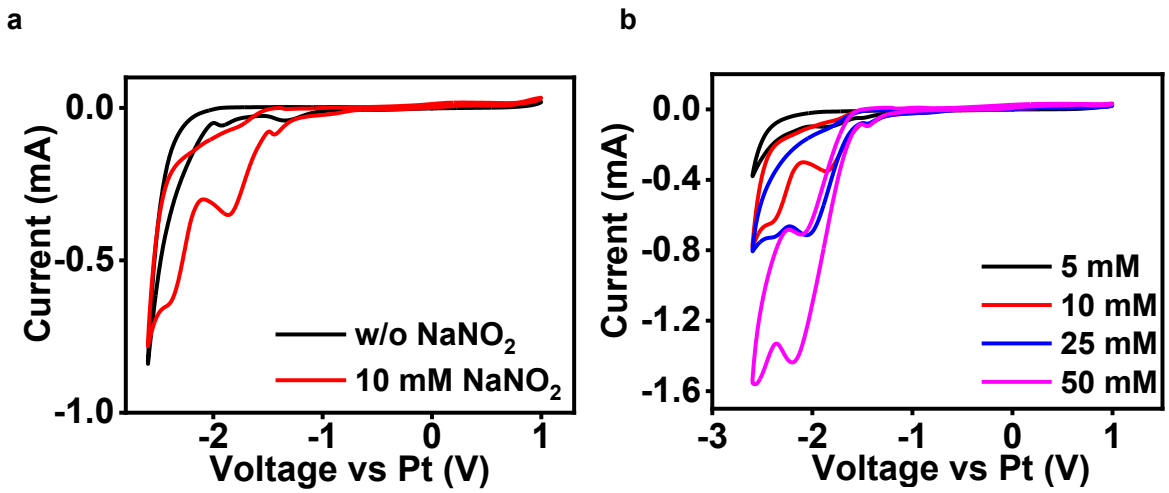

Figure S5. CV curves with different concentrations of $NaNO_2$ in Tyrode's solution.

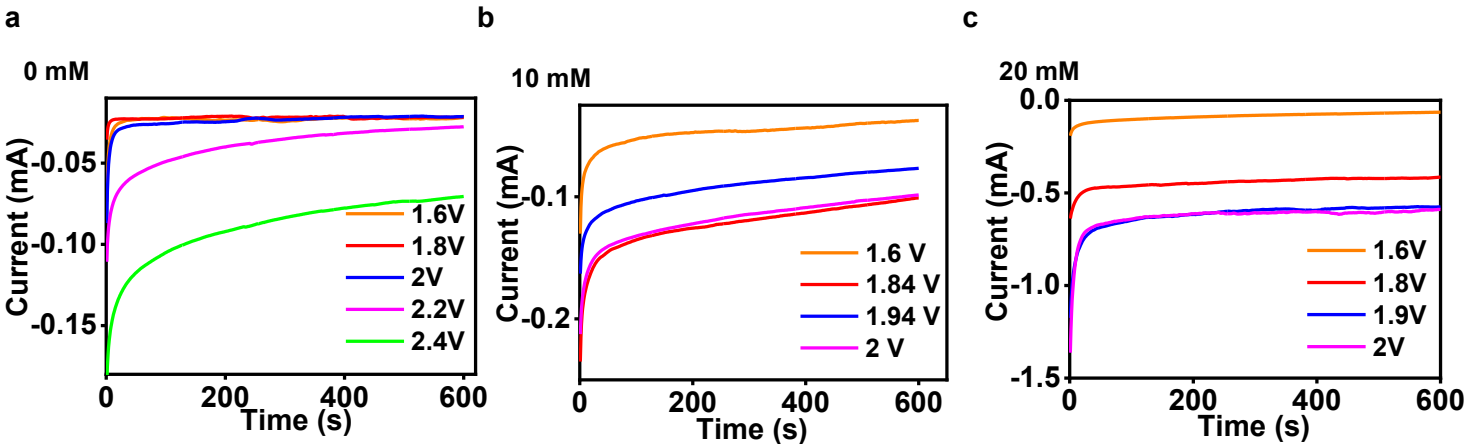

Figure S6. I-t curves of NO generation with different concentrations of $NaNO_2$ in Tyrode's solution. a, 0 mM. **b,** 10 mM. **c,** 20 mM.

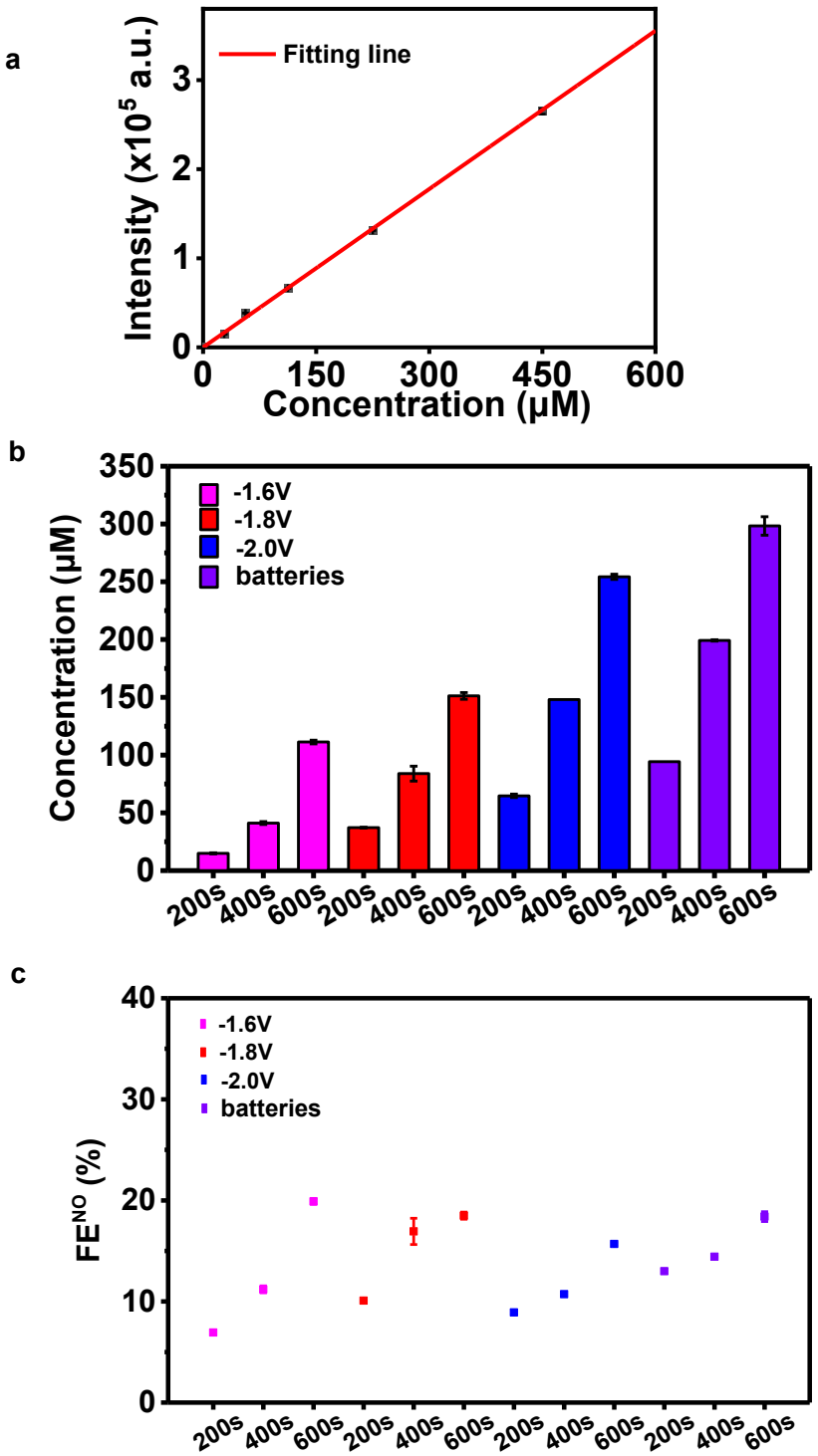

Figure S7. Characteristics of the electrochemical generation of NO. a, Calibration curve of NO quantification using DEA NONOate and DAF-FM. **b,** Electrochemical generation of NO driven by potentiostat and the Zn-Mo battery module. **c,** Corresponding calculated faradic efficiency (FE) of NO generation.

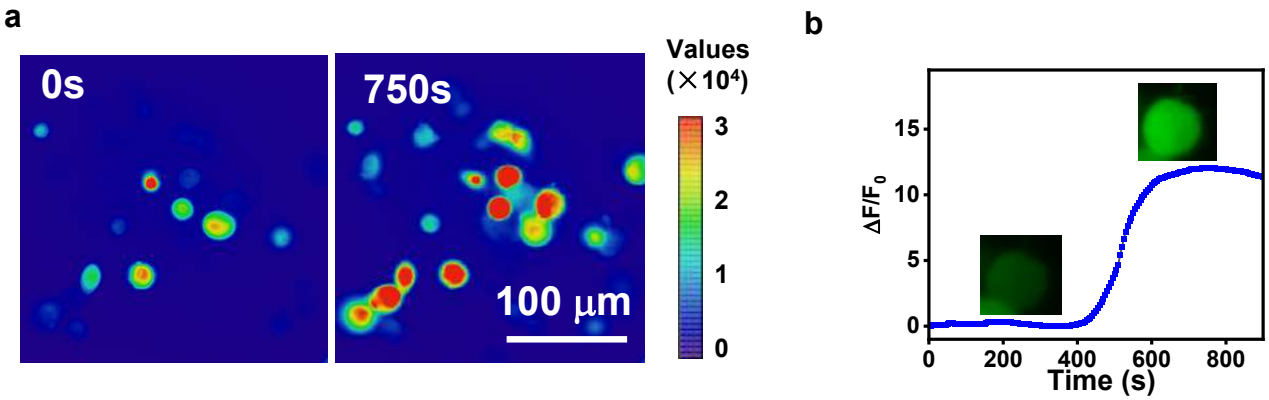

Figure S8. Representative fluorescent intensity changes in HEK cells triggered by NO generation driven by Zn-Mo batteries. a, Time-lapse images of Ca^{2+} responses in $TRPV1^{+}$ cells upon the production of NO by the Zn-Mo battery module. **b,** Representative trace of the fluorescent intensity of $TRPV1^{+}$ cell response to the production of NO. n = 3 independent experiments.

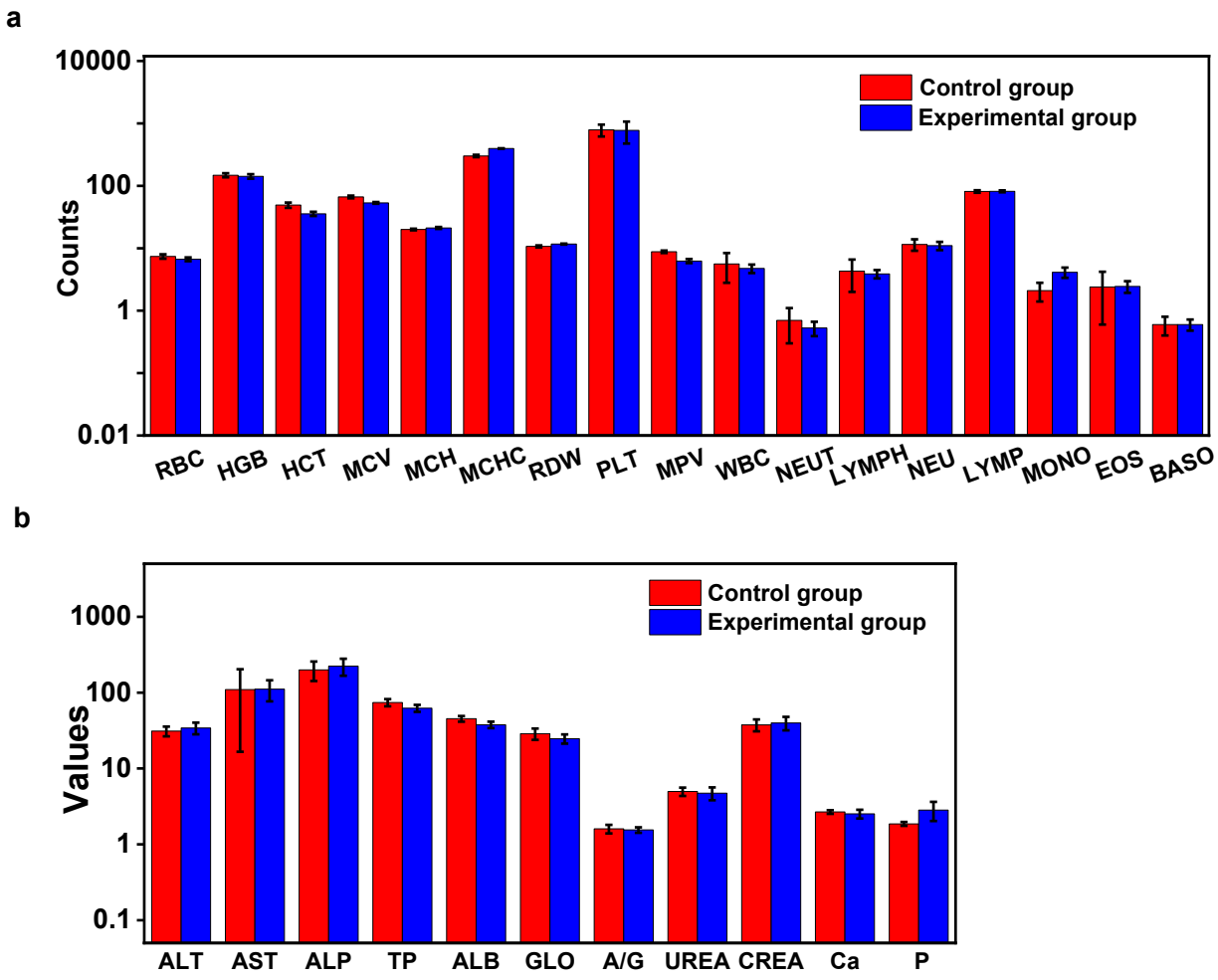

Figure S9. Hematology (a) and blood chemistry (b) analysis of SD rats implanted with Zn-Mo batteries (experimental group) and the control group. Abbreviations and corresponding units include, RBC: red blood cell (×1,000,000 μL^{-1}); HGB: blood haemoglobin level (g dL^{-1}); HCT: haematocrit level (%); MCV: mean corpuscular volume (fL); MCH: mean corpuscular haemoglobin (pg); MCHC: mean corpuscular haemoglobin concentration (g dL^{-1}); RDW: red cell distribution width (%); PLT: platelet count in blood (×1,000 μL^{-1}); MPV: mean platelet volume (fL); WBC: white blood cell (×1,000 μL^{-1}); NEUT: neutrophils (×1,000 μL^{-1}); LYMPH: lymphocytes (×1,000 μL^{-1}); NEU: percentage of neutrophils (%); LYMP: percentage of lymphocytes (%); MONO: percentage of monocytes (%); EOS: percentage of eosinophils (%); BASO: percentage of basophils ALT: alanine aminotransferase (U L^{-1}); AST: aspartate transaminase (U L^{-1}); ALP: alkaline phosphatase (U L^{-1});); TP: total protein (g dL^{-1}); : ALB: albumin (g dL^{-1}); GLO: globulin (g dL^{-1}); A/G: albumin to globulin ratio;); UREA: blood urea nitrogen (mg dL^{-1}); CREA: creatinine (mg dL^{-1}); Ca: calcium (mg dL^{-1}); P: phosphorus (mg dL^{-1}). n = 3 independent experiments. Data are represented as mean ± standard deviation.

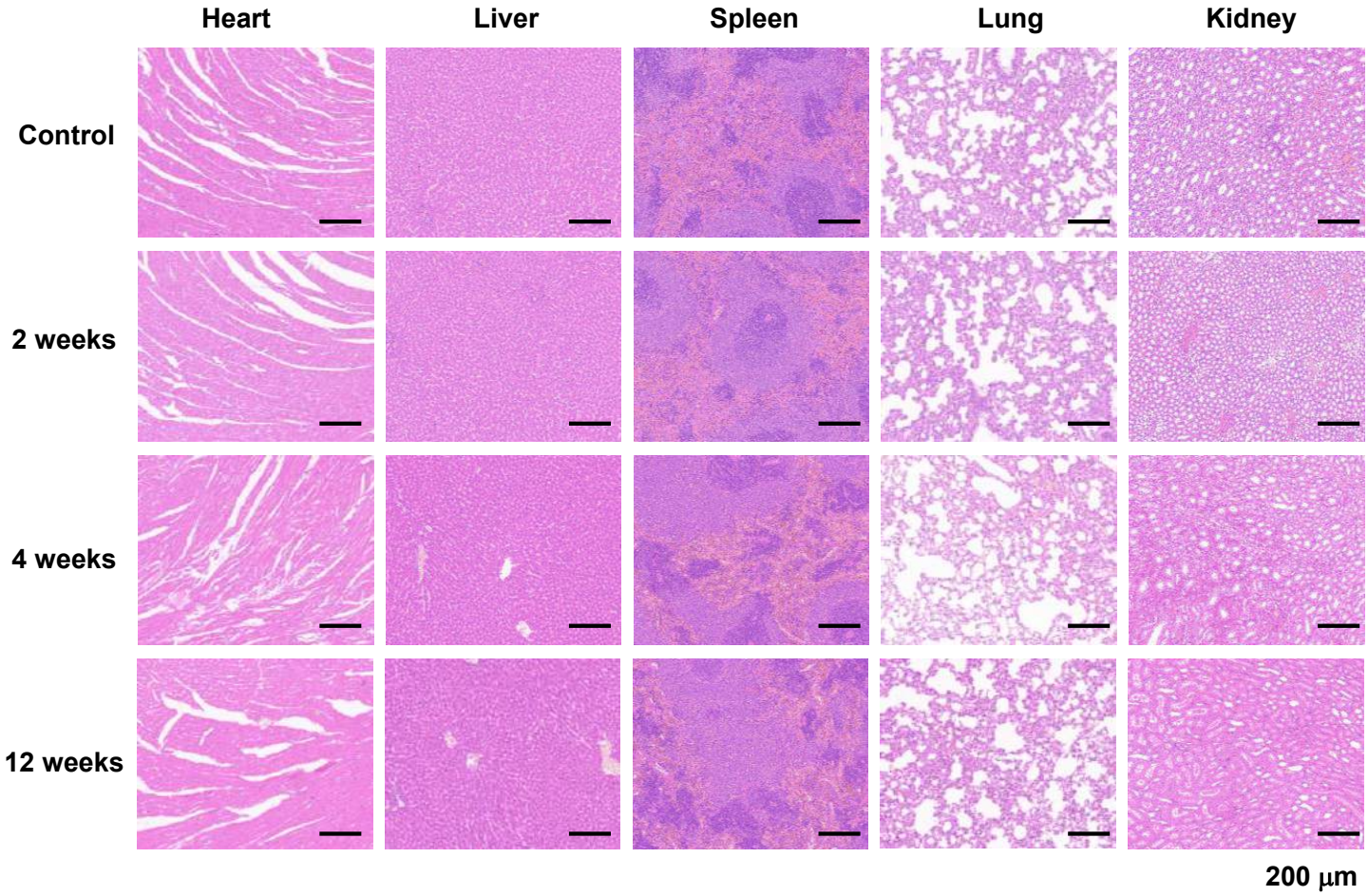

Figure S10. Hematoxylin and eosin (H&E) staining images of major organs of SD rats (heart, liver, spleen, lung and kidney) at different stages after the implantation of the Zn-Mo battery module. n = 3 independent experiments.

Table S1. Comparison of reported primary Zn biobatteries.

Materials	Electrolyte	Voltage (V)	Power (μW)	Lifetime	Energy capacity (μWh)	Degradability	Ref
Zn-Cu	Gastric juice	0.14	69	7 days	5796	Partial degradation	[1]
Zn-Pt	Gastric juice	0.6	300	40 mins	200	Partial degradation	[2]
Zn-Pd	Gastric juice	0.25	1250	1 h	1250	Partial degradation	[3]
Zn-Au	NaCl solution	0.55 (10 μA) 0.4 (30 μA)	5.5 12	200 h -	1100	Partial degradation	[4]
Zn-Mo	NaCl solution	0.7 (5 μA) 0.6 (10 μA)	3.5 6	19 days 12 days	1596 1728	Full degradation	**This work**

Table S2. Mechanical properties of electrodes, PLGA and gelatin electrolyte.

Materials	State	Young's Modulus (Mpa)
Gelatin	Hydrogel with 90% water content	0.024 [5]
PLGA	Dry film	0.012
Zn electrode	Dry film	0.251±0.092
Mo electrode	Dry film	0.509±0.267

Reference

[1] Nadeau, P.; El-Damak, D.; Glettig, D.; Kong, Y.L.; Mo, S.; Cleveland, C.; Booth, L.; Roxhed, N.; Langer, R.; Chandrakasan, A.P.; Traverso, G. Prolonged Energy Harvesting for Ingestible Devices. *Nat. Biomed. Eng.* **2017**, *1*.

[2] Jimbo, H.; Miki, N. Gastric-Fluid-Utilizing Micro Battery for Micro Medical Devices. *Sensors Actuators B: Chem.* **2008**, *134*, 219-224.

[3] Mostafalu, P.; Sonkusale, S. Flexible and Transparent Gastric Battery: Energy Harvesting from Gastric Acid for Endoscopy Application. *Biosens. Bioelectron.* **2014**, *54*, 292-296.

[4] Dong, Y.; Li, J.; Yang, F.; Wang, Y.; Zhang, Z.; Wang, J.; Long, Y.; Wang, X. Bioresorbable Primary Battery Anodes Built on Core-Double-Shell Zinc Microparticle Networks. *ACS Appl. Mater. Interfaces* **2021**, *13*, 14275-14282.

[5] He, Q.; Huang, Y.; Wang, S. Hofmeister Effect-Assisted One Step Fabrication of Ductile and Strong Gelatin Hydrogels. *Adv. Funct. Mater.* **2018**, *28*, 1705069.